Parametric Average Value Modeling of PWM DC-DC Converters

by

Ali Davoudi

B.Sc., Sharif University of Technology, 2003

A THESIS SUBMITTED IN PARTIAL FULFILMENT OF

THE REQUIREMENTS FOR THE DEGREE OF

MASTER OF APPLIED SCIENCE

in

THE FACULTY OF GRADUATE STUDIES

(Electrical Engineering)

THE UNIVERSITY OF BRITISH COLUMBIA

Jan. 2005

ABSTRACT

State-space average value modeling of hard switching PWM converters in continuous and discontinuous conduction modes has received significant attention in the literature and various models have been derived. In this thesis, a new approach for generating the average value model is set forth in which the parasitic effects of circuit elements are readily included. In the proposed methodology, the so-called duty ratio constraint and correction term are extracted numerically using the detailed simulation and expressed as nonlinear functions of the duty cycle and the average value of fast state variable. The proposed methodology is also generalized by representing these numerical functions in terms of duty cycle and the switching-cell dynamic-impedance. An automated small-signal characterization method using a general purpose simulator is also proposed. The resulting parametric average value model is compared with the hardware prototype, the detailed simulation and the analytically averaged model. The proposed model is shown to be very accurate in predicting large-signal time-domain transients as well as small-signal frequency-domain characteristics.

Table of contents

List of Tables

List of Figures

Acknowledgments

I would like to express my gratitude to Dr. Juri V. Jatskevich for his honest guidance, invaluable supervision, and financial support. I sincerely thank Dr. William Dunford, Dr. Joseph Yan, Dr. Patrik Palmer, and Dr. Jose R. Marti for their useful comments and serving on my thesis committee which have improved the quality of this thesis.

This work could not be accomplished without encouragement, discussion, and technical support of the graduate students in the Power Systems Simulation Lab. In particular: Dr. Khosro Kabiri, Hee-Sang Ko, Tarek Aboul-Seoud, and Tom De Rybel.

I would like to express my outmost gratitude to my beloved mother, to whom I am deeply indebted for her unconditional love and invaluable support.

CHAPTER 1

Introduction

1.1 PWM DC-DC Converters

The filed of power electronics is concerned with processing of electrical power using electronic devices, wherein the key module is the switching converter. Switching converters are traditionally classified based on their functionality (ac-dc, dc-dc...). Dc-dc power converters are employed in variety of applications associated with diverse power levels, including power supplies for personal computers, office equipments, appliance control, telecommunication equipments, dc motor drives, automotive, aircrafts, etc. In particular, dc-dc converters are often used as an interface between different dc levels. In dc-dc converter, input voltage is converted to larger or smaller output voltage, possibly with opposite polarity with or without isolation of input and output. The converter switching control is sometimes referred to as modulation, and a common modulation technique is Pulse Width Modulation (PWM). PWM is usually a simple pulse train resulted from a comparison between a reference waveform and a sawtooth or a triangular carrier waveform. This thesis specifically covers a class of lumped-parameter, hard-switching, non-isolated, unidirectional, fixed-frequency, PWM dc-dc converters. Properties, systematic synthesis, and classification of this class of converters are formulated in various literature sources, i.e. [1] - [6].

1.2 Computer Aided Simulation of Switching Converters

Computer aided modeling and simulations are essential stages of the analysis and design of power electronic systems, providing insight about the circuit operation. Using information provided by the numerical simulation, one can, for a given set of specifications, select appropriate circuit component types and values, estimate circuit performance, and complete the design by ensuring that the circuit performance will meet specifications even with the anticipated variations in operating conditions and circuit parameters.

There are numerous computer packages commonly used to simulate and analyze power electronic converters. Although each package provides unique features, they can be grouped into two general categories. In the first category, namely "state-variable-based", the system is described by differential equations, formulated as a set of state equations. These state equations are then solved numerically using well-known numerical algorithms for ordinary differential equations (ODEs) provided by the corresponding software. In the second category, namely "nodal-analysis-based", the system is described by circuit elements, branch parameters, and topology. Based on a particular integration algorithm such as trapezoidal or backward Euler, the difference equations are developed for each branch, relating the branch voltage and current vectors at a given instance to their values at previous instances.

The nodal analysis approach doesn't establish composite system state equations; therefore it doesn't provide system-level information and the implementation of various control schemes is not trivial. Consequently numerous analytical tools for stability analysis (eigenvalue-based, Lyaponouv-based), control schemes (pole-place, sliding mode control [7], nonlinear state feedback controller [8], control optimization), and model-order reduction [9] based on state-space description of a system are not applicable.

1.3 Operational Modes

The operational modes of a complex switched circuit can be identified based upon the cyclically repeated sequence of topologies that are observed during steady-state operation. The analytical derivation of operating mode boundaries is limited to low order dc-dc converters. In general cases, computer aided methods are developed to determine the operating mode boundaries mostly by solving the nonlinear algebraic equations for boundary conditions [10], [11]. The set of all possible operating modes may not be known, and the analytical derivation of boundary equations is not trivial. An automated algorithm is represented in [12], where operational modes are identified in term of the minimal repetitive subsequence of switching state and the number of state variables in each switching state.

The concept of operational modes is illustrated using an example of buck converter with input filter shown in Fig. 1.1(a). All four possible topological instances are shown in Fig. 1.1(b). Potential repeated sequences of topologies and corresponding operational modes are represented as well.
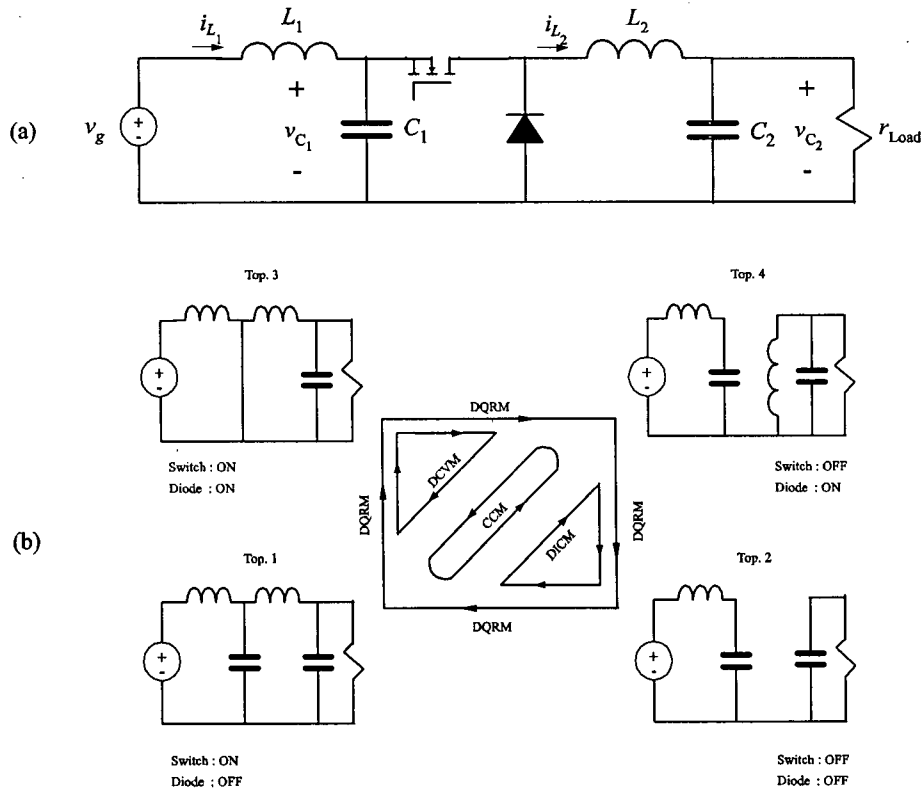
Fig. 1.1: (a) Buck converter with input filter; (b) Possible topological instances and operational modes

For this type of converters, the most common operational mode is the continuous conduction mode (CCM), whereas two topologies Top. 2 and Top. 3 are sequentially repeated within a prototypical switching interval. In this mode, the diode switching is synchronized with the active switch; when the active switch is on, the diode is off and vice versa[1].

For the given topology, it is possible to have both switch and diode off simultaneously which results in the inductor current i_{L_1} being clamped to zero. This operational sequence has been refereed to as discontinuous inductor current mode (DICM). DICM is the most frequently encountered discontinuous conduction mode in PWM dc-dc converters. Therefore, emphasize of this thesis is mainly on average value modeling of dc-dc converters in DICM.

The discontinuous capacitor voltage mode (DCVM)[2] is concluded by considering duality of DICM. If the capacitor, the active switch, and the diode are connected in a loop, it is possible for the capacitor voltage v_C to be clamped to zero by having both switches simultaneously on.

The discontinuous quasi-resonant mode (DQRM) is constructed as combination of DCVM and DICM[3]. On one hand, the active switch is turned on at zero current and off at zero voltage. On the other hand, the diode is turned on at zero voltage and off at zero current. Despite the fact that switching frequency is constant in PWM converter, the PWM in DQRM behaves similar to various quasi-resonance converters [13].

In this thesis, a discontinuous conduction mode for a state variable x is considered as cyclically repeated sequence of topological instances such that at least in one of the topological instances, the derivative of the state variable x is zero and its dynamics disappears.

Discontinuous conduction mode occurs in switching converters with unidirectional current/voltage switches implemented, when the switching ripple of fast state variable is large enough to cause the polarity of switch current/voltage to reverse. This effect could be

---

[1] The operational mode of converters controlled to operate at the boundary of CCM and DCM is sometimes classified as boundary or critical conduction mode [14].

[2] Discontinuous capacitor voltage mode is sometime encountered in the input filter of the basic dc-dc converter (i.e. Buck converter) in single phase power factor correction converter. It has been referred as discontinuous input-voltage mode in [15].

[3] The combination of DICM and DCVM is sometimes called as double discontinuous conduction mode [16]. Most generally, a converter with several discontinuous state variables is operating in so-called multiple discontinuous mode [17].

4

encountered in a converter operating under a light load with large inductor current ripple. Discontinuous conduction mode is inevitable since converters often operate with their load removed. In fact, some dc-dc converters are purposely designed to operate in DCM for all loads [18] and [19]. For example, in low-power applications, it may be preferred to operate the converter in DCM even at full load in order to avoid reverse recovery problem of diode. DCM also yields faster transient responses.

In integrated high-quality rectifier regulator, the converter consists of boost integrated/fly back rectifier/energy storage/dc-dc converter (BIFRED) [20]. It has been demonstrated that DCM avoids the light-load high-voltage stress problem associated with BIFRED topologies in continuous conduction mode (CCM). Furthermore, DCM results in an improved power factor and simpler control loop structure in comparison to CCM [21]. Cuk derived high quality rectifiers [21] and power factor pre-regulators (PFP) [23] that are mainly implemented in discontinuous capacitor voltage mode (DCVM). This mode features unity power factor, zero voltage crossing at turn-off, low switch current stress, and reduction of reactive element values; while there is no need to modulate the duty cycle. The sepic converter in DICM also functions as PFP [24]. Resulted PFP is a voltage follower with adjustable current ripple in design stage while no current loop is necessary. In some topologies, double discontinuous conduction mode operation provides soft switching without utilizing additional snubber circuits [16]. In single phase ac/dc PWM converter with active power factor correction (PFC) the input inductor current becomes discontinuous in every half a "line-cycle" as the line voltage crosses zero. Some PFC circuits are even purposely designed to operate in DCM over the entire line cycle in order to simplify the control [25].

The steady-state and dynamic behaviors of two identical dc-dc converters are vastly different depending on their operating modes. For example, in CCM conversion ratio is controlled by duty cycle, while in DCM it is load-dependent as well as duty-controlled. The output impedance usually increases in discontinuous conduction mode. The conventional approaches to analysis the dc-dc converter in time and frequency-domain based on CCM assumptions are not valid for DCM. For the purposes of design and evaluation of steady-state and dynamic performance, accurate models of converters in DCM are needed.

5

1.4 Average Value Modeling

The detailed simulation of converters wherein the switching of each power electronic device is represented is computationally intensive. The complexity of detailed models also makes the simulation of large multi-converter power-electronic systems such as those in [26], [27] more time consuming.

The small- and large-displacement stability of systems with multiple converters is an important issue. There are various techniques for investigating stability of power-electronic-based systems and design of controllers that are based upon frequency-domain characteristics, for example [27]. The impedance characteristics can be extracted from a detailed model of the converter or from a hardware prototype. The traditional methods of extracting small-signal transfer-function include frequency sweep techniques [28] and injection of non-sinusoidal and possibly spike-like signals [29]. The later methods work well with linear systems, and the frequency sweep methods work well with both linear and nonlinear systems with or without switching. However, because the detailed models are computationally intensive, determining the impedance over wide range of frequencies, using a frequency sweep methods, is a time consuming procedure, particularly when it includes obtaining data points at very low frequencies (<10Hz).

These challenges led to the development of the so-called average value models wherein the effects of fast switching are neglected or "averaged" with respect to the prototypical switching interval and the respective variables are constant in steady-state. Although the resulting models are often nonlinear and only approximate the longer-term dynamics of the original systems, the average value models are continuous and, therefore, can be linearized around a desired operating point. Many simulation programs offer automatic linearization and subsequent state-space and/or frequency-domain analysis tools [30], [31]. Thereafter, obtaining a local transfer-function and/or frequency-domain characteristics becomes a straightforward and almost instantaneous procedure. Moreover, it has been shown in [32] that the asymptotical stability of the average value model and that of detailed switching circuit are equivalent. Therefore, the calculated transfer-functions may be used to design and optimize the associate controllers. Additionally, the average value models typically execute orders of magnitude faster than the corresponding detailed models making them ideal for representing the respective components in system-level studies.

Numerous methods have been developed for the average value modeling of PWM dc-dc converters in discontinuous conduction mode; among them reduced-order state-space averaging [33], reduced-order averaged-switch modeling [1], equivalent duty ratio model [34], loss-free resistor model [35], full-order averaged-switch modeling [36], and full-order state-space averaging [37]. Average value models may be categorized by resulting systems of equations (reduced-order vs. full-order); or by derivation methodology (sampled data modeling, circuit averaging, state-space averaging). Both full-order as well as reduced-order models can be obtained by averaging approaches including sampled data modeling, circuit averaging or state-space averaging. The conventional reduced-order models treat the discontinuous variable as a dependent variable and eliminate its dynamic from state equations. It may seem that the reduced-order models should provide accurate step response, since the discontinuous variable vanishes within switching cycle. However, despite the correct dc-analysis and low-frequency match, large discrepancies especially in phase response are observed in frequencies higher than one-tenth of switching frequency [37]. Also the elimination of fast/discontinuous state variable is undesirable for application in which this variable is used for control purpose. The methods based on equivalent duty ratio, full-order averaged-switch modeling, and loss-free resistor methods generate the average value models that retain the "missed" state variable and have shown great improvements over the reduced-order models.

One approach to eliminate the discontinuity of the system equations is through sampled data modeling [38]-[41]. The main goal there is to suppress the internal details of a switching cycle, focusing instead on a cycle-to-cycle behavior. In the basic model [42], a sample of the state variables at each switching period is related to the sample of the control inputs in the same switching period and the sample of the state variables in the previous switching periods. The states evolution for switched network can be described very easily using standard matrix exponential expression for LTI systems, and trajectories in each segment can then be pieced together by invoking the continuity of the state variables. The sampled-data models are easily recognize as forward-Euler approximation of state-space averaged models, obtained by replacing the derivation by a formal difference. Since the sampled data modeling neglects the dynamics of state variables between sampling instances, deficiencies arise in predicting the high-frequency dynamics [43], [44]. Therefore their application is mostly limited to study and control of ripple instabilities and mixed-signal control of switching converters.

7

First introduced in [45], the so-called circuit averaging (also known as in-place averaging [46] or direct averaging [47]) attempts to replace each element in switching converter with an appropriate "averaged element". The extension of circuit averaging is the averaged-switch modeling which has received significant attention in the literature i.e. [1], [14], [35], [36], [48] - [52]. Since the switching characteristics of converter waveforms are due to the converter switch-network, to obtain a time-invariant circuit topology, the switch-network ports are replaced with averaged voltage and current sources.

The essential step in averaged-switch modeling is to identify a switching-cell [1] (also known as converter-cell [53]) that is common in different topologies and to develop an equivalent circuit that, when inserted in place of the original switching-cell, results in an electrical circuit that has the same average behavior as the original converter. An equivalent switch-averaged model of the switching-cell in DCM is a three-terminal static network with algebraic relations between its terminal variables. The inductor has been considered in switching-cell while the equivalent averaged-switching-cell is a static network. Full-order averaged-switch models are established by excluding the inductor from the static network, for example in [36], [37]. Also, the averaged-switch models are the suitable candidates for nodal-analysis-based simulation of the switching converters. However, circuit averaging doesn't realize the elements required to replace the switch-network. A so-called hybrid modeling is investigated in [54], where the obtained averaged circuit model is a realization of the original state-space averaged model. The identification of switch-network is not trivial and since a new switch average model is necessary for different configurations of switch-network, averaged-switch modeling is difficult to automate.

State-space averaging is based on the classical averaging theory and involves manipulation of state-space equations of a converter system. First, a state-space representation of converter is obtained for each subinterval. Then, the obtained piece-wise linear equations are weighted by the corresponding subinterval length and added together. Conditions for state-space averaging are characterized by linear and/or small ripple approximation [48] and the degree to which certain vector fields commute [55] (see Appendix A). With small ripple approximation, the Fourier series expansion for a finite length segment of a circuit waveform is dominated by its DC term. With linear ripple approximation, the circuit waveform appears as linear function of time when examined over switching subintervals.

The application of classical averaging to PWM converters is studied in [45]. It has developed an asymptomatic framework where solutions to switched systems (including large ripples) has been approximated to arbitrary accuracy by a power series in small parameter ε. The small parameter ε is determined as a function of switching period and systems time constants. In general case of switching converters, the averaging is formulated as generalized state-space averaging ([56] - [59]) by interpreting dynamic phasors as state variables. State-space averaging has been demonstrated to be an effective method to analyze PWM converters. Analytical averaging, however, is based on a so-called small-ripple approximation and the derivation methods are challenging. Most of previous averaging efforts were in derivation for a specific ideal topology. In addition, in the derivation of state-space average value model, the equivalent series resistance (ESR) of circuit components are often neglected and the state variables are considered as linear segments. Such assumptions result in inaccuracy of the corresponding time constants as well as the waveforms. If the losses due to the switch and/or inductor are taken into account, whereby the linear shape of the current waveform would change into exponential form, the analytically derived models would become more complicated. The analytical derivation also becomes more complicated when the number of energy storage elements is increased and/or the fast state variable is held at a nonzero constant value within the third subinterval [60].

1.5 Automated Small-Signal Characterization of Switching Converters

Numerous analytical and numerical techniques have been developed for small-signal frequency-domain analysis of power electronic converters. Frequency-domain characterization is most commonly obtained via perturbation and linearization of continuous models (ac models) or via sampled-data models, which are now well described in textbooks, i.e. [35],[61]-[63], as well as more accurate and general but more complex models (such as [17],[43],[64]-[66]). In practice, there are often configurations, control methods, or operating modes where appropriate analytical continuous small-signal models are not available and/or difficult to derive. Consequently, automated computer-aided small-signal characterization of switching converters is indispensable.

Limitations of basic sampled-data models in predicting small-signal frequency responses have been pointed out in [43] and [44]. The resulted mismatches in the predicted transfer-functions illustrate the importance of taking into account not only sampling of the control inputs, but also the continuous nature of the converter outputs, in particular, the responses of the converter state variables between samples. In reduced-order average value models [33], [37], [50], [67], [68], the high-frequency pole and resulted phase lag and magnitude reduction are not predicted, which can be significant even at relatively low frequencies. In the continuous-time full-order average value models inheriting the volt-second balance over inductor ([34], [36]), the averaged model clearly over-estimate the phase lag and the drop in the magnitude introduced by the inductor dynamics. The full-order average value model with the duty ratio constraint defined as the function of fast state variable ([34], [35], [37], [48], [50], [69], and [70]) is the most accurate model to give frequency-domain results identical to the ones obtained from detailed model and the hardware. However, derivation is limited to the specific ideal topologies. The analytical derivation of average value model is cumbersome; some automated computer aided schemes are proposed to extract the small-signal transfer-function from detailed switching converter without averaging, i.e. [71], [73], [74].

An automated small-signal frequency-domain analyzer is described in [71] based on an algorithm similar to the algorithms presented in [43], [65], [66]. In this algorithm, steady-state time-domain solution (named "small-signal steady-state") is found for the case when inputs have one or more small-signal sinusoidal sources on top of the large-signal, steady-state waveforms. However, the algorithm is based on the superposition principle, which is suitable only for linear

10

networks. The steady-state derivation is tied to the algorithm described in [72] and the model implementation is tied to a special-purpose switched-circuit simulator.

In [73], small-signal transfer-function of switching converters is obtained using the system identification techniques. A pseudorandom perturbation signal with the spectrum spanning the entire range of frequencies of interest is added to a pre-set input. The system is then simulated in time-domain using a general-purpose simulator to generate output responses. Finally, the simulation results are used as inputs to the identification algorithm to determine parameters in a small-signal model of a required order. The approach obtains accurate frequency responses using results from a time-domain general-purpose simulator, but is empirical in nature, and may require experimenting with the assumed system order, perturbation signal or length of simulation.

The most accurate small-signal characterization method based on impulse responses of dc-dc converters is introduced in [74]. The converter impulse response obtained from Pspice or PETS [75] is analyzed in the mathematica over a few cycles. The mathematica updates the circuit netlist file with the initial values for state variable, and launches the simulator to obtain state variable over switching period. The laplace transform of the impulse transient data generates the small-signal frequency response in mathematica. Since the responses are obtained using the numerical time-domain simulation, the converter model need not to be piecewise linear, and can include any complex nonlinear converter configuration supported by the general-purpose simulator. However, this automated method is facilitated to obtain only the control-to-output small-signal transfer-function. Also, the interaction algorithm is language dependent (SPICE or SPICE derivative simulators). The derivation of steady-state initial condition is tied to the algorithm in [76]. To evaluate the transition matrix, n+1 simulation runs are necessary (n-number of state variables). Since this scheme doesn't provide a continuous-time model to linearize, the computationally intensive process should be repeated each time a new control-to-output transfer-function is sought.

In this thesis, an alternative method for constructing the average value models is proposed. First, it is shown how the conventional state-space averaged equation can be corrected in order to include the fast dynamics of the discontinuous state variables. The correction matrix is formulated and diagonalized to decouple correction for each state variable. The key point

11

includes introducing the correction terms and conduction intervals as numerical functions of the so-called switching-cell dynamic-impedance that results in accurate full-order average value models. An automated small-signal characterization procedure is set forth for frequency-domain analysis. Because the correction term and the duty ration constraint are obtained numerically from the detailed simulation, the effect of circuit parasitics and nonlinearities of waveforms is readily incorporated into the final model. The proposed methodology is demonstrated on basic converters and is readily extendable to other topologies. The accuracy of the generated average value model has been verified in time as well as frequency-domain against the hardware prototype, the detailed simulation, and the analytically derived averaged model.

CHAPTER 2

State-Space Average Value Modeling

2.1 General Framework

Switched converters are often modeled as piece-wise linear networks wherein the topology changes at the boundaries between the subsequent subintervals within a prototypical switching cycle [77]. The state variables are typically associated with the energy storage components. Based on the topological state of each switching element such as transistor and diode, appropriate state-space equations can be established. The state-space model notion and the procedure to derive it from circuit topology are explained for example in [62]. In addition, there are well-defined algorithms [78] and software tools [79], [80] wherein the state-space model is generated automatically and updated dynamically for each new topological state of the system studied. Regardless of the approach/tool used, inside each k-th subinterval, the system state model may be expressed by the system matrices, herein denoted by $\mathbf{A}_k$, $\mathbf{B}_k$, $\mathbf{C}_k$ and $\mathbf{D}_k$.

The most common dc-dc converters include boost, buck and buck-boost topologies. Higher order converters are built from these basic converters by cascading (Spiec, Zeta, Cuk) or by including an isolation transformer (PFC converters, fly back converters) [81]. Therefore, analysis of basic dc-dc converters has justifiably received significant attention in the literature. As a representative of basic topologies, a boost is shown in Fig. 2.1(a). Buck and buck-boost topologies can be derived from the boost converter by rotating the switching cell consisting of an inductor, a switch and a diode.
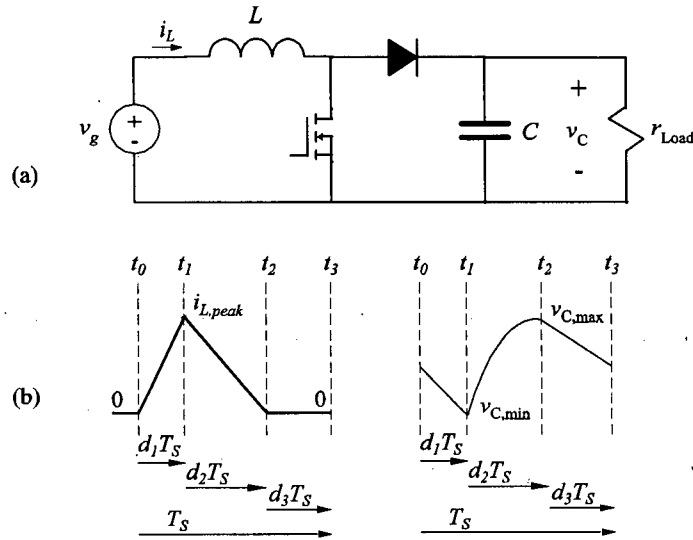
Fig. 2.1: (a) Boost converter circuit diagram; (b) state variables waveform in DCM

The boost converter dynamic behaviour is determined by its state variables and input signals. Although each set of linearly independent variable can be chosen as state variables, it is convenient to adopt the inductor current and capacitor voltage as the state variables. In comparison to the fast dynamic response of inductor current, the capacitor voltage typically undergoes slower dynamic transient and usually remains continuous. Thus, in the given topology, the inductor current and capacitor voltage may be called the fast and slow state variables, respectively. Slow state variables usually stay continuous while fast state variables may be continuous or discontinuous. If both inductor current and capacitor voltage are continuous, then the converter operates as a controlled voltage source. In continuous conduction mode, a prototypical switching interval is divided into two subintervals ($k = 1,2$), (t_0, t_1) and (t_1, t_2), and the respective duty cycles are d_1 and $d_2 = 1 - d_1$. It is assumed that the duty cycle of the active switch d_1 is controlled externally.

2.2 State-Space Averaging

The state-space averaging of continues conduction mode has been presented previously in numerous publications, for example [35], [67], [68], and [82]. The converter's switched state-space model in this mode is

$$\dot{\mathbf{x}}(t) = (q(t)\mathbf{A}_1 + (1 - q(t))\mathbf{A}_2)\mathbf{x}(t) + (q(t)\mathbf{B}_1 + (1 - q(t))\mathbf{B}_2)\mathbf{u}(t) \tag{1}$$

where $q(t)$ is the switching function, $\mathbf{A}_i, \mathbf{B}_i$ are the system matrices, and $\mathbf{u}(t)$ is an input vector. The so-called fast average of a state variable $x(t)$ over a switching interval is

$$\bar{x}(t) = \frac{1}{T_s} \int_{t-T_s}^{t} x(\tau) d\tau \tag{2}$$

The resulted $\bar{x}(t)$ is also called the actual or the true average of $x(t)$. Since

$$\dot{\bar{\mathbf{x}}}(t) = \frac{d}{dt} \frac{1}{T_s} \int_{t-T_s}^{t} x(\tau) d\tau = \frac{\mathbf{x}(t) - \mathbf{x}(t - T_s)}{T_s} = \frac{1}{T_s} \int_{t-T_s}^{t} \dot{\mathbf{x}}(\tau) d\tau = \bar{\dot{\mathbf{x}}}(t) \tag{3}$$

the averaging operator is commutative with respect to differentiation operator. Taking the fast average of (1) over a prototypical switching interval results in

$$\dot{\bar{\mathbf{x}}}(t) = (d(t)\mathbf{A}_1 + (1 - d(t))\mathbf{A}_2)\bar{\mathbf{x}}(t) + (d(t)\mathbf{B}_1 + (1 - d(t))\mathbf{B}_2)\mathbf{u}(t) \tag{4}$$

This is a straight conclusion of the fact that the fast average of switching function over a prototypical switching interval is what is called the duty cycle function

$$d(t) = \frac{1}{T_s} \int_{t-T_s}^{t} q(\tau) d\tau \tag{5}$$

Another assumption made here is that the average of the product is equal to the product of the averages. Specifically,

$$\overline{\mathbf{Bu}} = \overline{\mathbf{B}} \cdot \overline{\mathbf{u}} \tag{6}$$

$$\overline{\mathbf{Ax}} = \overline{\mathbf{A}} \cdot \overline{\mathbf{x}} \tag{7}$$

Eq. (6) is usually true when the source ripple is neglected. Eq. (7) is acceptable if the original switching variables don't deviate significantly from their average values (small ripple

approximation) and system matrices $\mathbf{A}_1$ and $\mathbf{A}_2$ are commutative [82], [also, see Appendix A]. These assumptions are generally appropriate for the case of high-frequency converters working in continuous conduction mode.

Since there is a common node between the switch, the diode and the inductor, it is possible for the inductor current i_L to be clamped to zero by having both switch and diode off simultaneously. This phenomenon results in discontinuous conduction mode. The inductor current i_L and the capacitor voltage v_C in this mode are shown in the Fig. 2.1(b). In the case of a boost converter operating in discontinuous conduction mode, there are three topological states ($k = 1,2,3$). In this mode, a prototypical switching interval is divided into three subintervals corresponding to d_1, d_2, and $d_3 = 1 - d_1 - d_2$, respectively. Herein, d_2 becomes a dependent variable which now can be expressed as an algebraic function of other variables of the system. This dependency of d_2 is frequently called the duty ratio constraint [35], [37].

State-space averaging for converters working in discontinues conduction mode has been summarized for example in [37] and [50]. For this mode, the direct extension of (1)-(4) results in

$$\dot{\mathbf{x}} = (d_1 \mathbf{A}_1 + d_2 \mathbf{A}_2 + d_3 \mathbf{A}_3)\bar{\mathbf{x}} + (d_1 \mathbf{B}_1 + d_2 \mathbf{B}_2 + d_3 \mathbf{B}_3)\mathbf{u} \qquad (8)$$

which is not accurate anymore. The conventional state-space averaging method in (8) averages only the system matrices and not necessarily the state variables. To see this, one should consider a fast state variable (inductor current) which is clamped to a constant value in the third subinterval. The simplifying assumptions made in (7) represent a problem in discontinuous conduction mode. In particular, in the third subinterval, the actual average of the discontinuous state variable is zero as i_L is zero [see Fig. 2.1(b)], whereas the conventional state-space averaging implies that the local average value of i_L in the subinterval (t_2, t_3) is $d_3 \bar{i}_L$. Therefore, in this mode, the conventional state-space averaging and the actual averaging arrive at different results. Since $\bar{i}_L$ is not zero, the result out of conventional state-space averaging is not zero unless the length of discontinuous subinterval d_3 is zero, which is true in continuous and/or boundry conduction mode. This example shows the inconsistency of conventional state-space averaging in discontinuous conduction mode. Another example of such inconsistency in terms of predicting the capacitor charging current is given in [37].

16

2.2.1 Correction term

In order to obtain a correct state-space averaged equation one should consider the true averaging from the very beginning. To do that, it is instructive to partition the state vector $\mathbf{x}$ within the prototypical switching interval T_s as $\mathbf{x} = \mathbf{x}_1 + \mathbf{x}_2 + \mathbf{x}_3$ corresponding to each subinterval. In particular,

$$\mathbf{x}_1(t) = \begin{cases} \mathbf{x}(t) & 0 \le t \le d_1 T_s \\ 0 & \text{Elsewhere} \end{cases} \tag{9}$$

$$\mathbf{x}_2(t) = \begin{cases} \mathbf{x}(t) & d_1 T \le t \le (d_1 + d_2)T_s \\ 0 & \text{Elsewhere} \end{cases} \tag{10}$$

$$\mathbf{x}_3(t) = \begin{cases} \mathbf{x}(t) & (d_1 + d_2)T_s \le t \le T_s \\ 0 & \text{Elsewhere} \end{cases} \tag{11}$$

The corresponding state models are

$$\dot{\mathbf{x}}_1(t) = \begin{cases} \dot{\mathbf{x}}(t) = \mathbf{A}_1 \mathbf{x}(t) + \mathbf{B}_1 \mathbf{u} & 0 \le t \le d_1 T_s \\ 0 & \text{Elsewhere} \end{cases} \tag{12}$$

$$\dot{\mathbf{x}}_2(t) = \begin{cases} \dot{\mathbf{x}}(t) = \mathbf{A}_2 \mathbf{x}(t) + \mathbf{B}_2 \mathbf{u} & d_1 T_s \le t \le (d_1 + d_2)T_s \\ 0 & \text{Elsewhere} \end{cases} \tag{13}$$

$$\dot{\mathbf{x}}_3(t) = \begin{cases} \dot{\mathbf{x}}(t) = \mathbf{A}_3 \mathbf{x}(t) + \mathbf{B}_3 \mathbf{u} & (d_1 + d_2)T_s \le t \le T_s \\ 0 & \text{Elsewhere} \end{cases} \tag{14}$$

By applying formal averaging to both sides of (12)-(14) the so-called local average models are produced. For example, in the first subinterval (12) implies

$$\dot{\bar{\mathbf{x}}}_1 = \frac{1}{T_s} \int_0^{d_1 T_s} (\mathbf{A}_1 \mathbf{x}(\tau) + \mathbf{B}_1 \mathbf{u}) d\tau \tag{15}$$

Since $\mathbf{A}_1$ and $\mathbf{B}_1 \mathbf{u}$ terms are constant, and

$$\frac{1}{T_s} \int_0^{d_1 T_s} \mathbf{x}(\tau) d\tau = \frac{1}{T_s} \int_0^{T_s} \mathbf{x}_1(\tau) d\tau = \bar{\mathbf{x}}_1, \tag{16}$$

we get

$$\dot{\bar{\mathbf{x}}}_1 = \mathbf{A}_1 \bar{\mathbf{x}}_1 + d_1 \mathbf{B}_1 \mathbf{u} \tag{17}$$

Applying the same procedure to (13) and (14) results

17

$$\begin{cases} \dot{\bar{\mathbf{x}}}_1 = \mathbf{A}_1 \bar{\mathbf{x}}_1 + d_1 \mathbf{B}_1 \mathbf{u} \\ \dot{\bar{\mathbf{x}}}_2 = \mathbf{A}_2 \bar{\mathbf{x}}_2 + d_2 \mathbf{B}_2 \mathbf{u} \\ \dot{\bar{\mathbf{x}}}_3 = \mathbf{A}_3 \bar{\mathbf{x}}_3 + d_3 \mathbf{B}_3 \mathbf{u} \end{cases} \tag{18}$$

The final averaged system-equation is obtained from (18) as

$$\dot{\bar{\mathbf{x}}} = \dot{\bar{\mathbf{x}}}_1 + \dot{\bar{\mathbf{x}}}_2 + \dot{\bar{\mathbf{x}}}_3 = (\mathbf{A}_1 \bar{\mathbf{x}}_1 + \mathbf{A}_2 \bar{\mathbf{x}}_2 + \mathbf{A}_3 \bar{\mathbf{x}}_3) + (d_1 \mathbf{B}_1 + d_2 \mathbf{B}_2 + d_3 \mathbf{B}_3) \mathbf{u} \tag{19}$$

Equation (19) can be rewritten as

$$\dot{\bar{\mathbf{x}}} = (d_1 \mathbf{A}_1 \mathbf{W}_1 + d_2 \mathbf{A}_2 \mathbf{W}_2 + d_3 \mathbf{A}_3 \mathbf{W}_3) \bar{\mathbf{x}} + (d_1 \mathbf{B}_1 + d_2 \mathbf{B}_2 + d_3 \mathbf{B}_3) \mathbf{u} \tag{20}$$

where the diagonal weighing-correction matrix is $\mathbf{W}_k = diag[\omega_{k1}, \omega_{k2}]$ with the entries defined as

$$\omega_{kj} = \mathbf{W}_k(j, j) = \frac{\bar{\mathbf{x}}_k(j)}{d_k \bar{\mathbf{x}}(j)} \tag{22}$$

Here, since the actual average of discontinuous state i_L in the third subinterval is zero, the correction coefficient ω_{31} is zero as defined by (21). Finally, by analyzing (7) and (20), a so-called correction matrix can be defined as

$$\mathbf{M} = \left[\sum_{k=1}^{3} d_k \mathbf{A}_k \right]^{-1} \cdot \left[\sum_{k=1}^{3} d_k \mathbf{A}_k \mathbf{W}_k \right] \tag{22}$$

whereas the corrected state-space averaged equation can be expressed as

$$\bar{\mathbf{x}}(t) = (d_1 \mathbf{A}_1 + d_2 \mathbf{A}_2 + d_3 \mathbf{A}_3) \mathbf{M} \bar{\mathbf{x}}(t) + (d_1 \mathbf{B}_1 + d_2 \mathbf{B}_2 + d_3 \mathbf{B}_3) \mathbf{u}(t) \tag{23}$$

This is similar to the analytical derivation in [37] where $\mathbf{M}$ is also a diagonal matrix. In particular, in [37] the inductor current i_L has a triangular waveform, and the diagonal entries corresponding to i_L and v_C have been found to be $\dfrac{1}{d_1 + d_2}$ and 1, respectively. As it is summarized in Table 2.1, the first diagonal entry is obtained by comparing the actual charging current of the capacitor with the results of the corresponding state-space averaged model. The second diagonal entry is assumed 1, since capacitor voltage is continuous and small ripple assumption is made.

Table 2.1: Charging of capacitor by an inductor operating in DCM [37]

Inductor charging current	State-space averaged equivalent charging current	Actual equivalent charging current
When the active switch is on	$\bar{i}_L \cdot d_1 = \dfrac{i_{L,peak} \cdot d_1}{2} \cdot (d_1 + d_2)$	$\dfrac{i_{L,peak} \cdot d_1}{2}$
When the active switch is off	$\bar{i}_L \cdot d_2 = \dfrac{i_{L,peak} \cdot d_2}{2} \cdot (d_1 + d_2)$	$\dfrac{i_{L,peak} \cdot d_2}{2}$
Over the entire cycle	$\bar{i}_L \cdot (d_1 + d_2) = \dfrac{i_{L,peak}}{2} \cdot (d_1 + d_2)^2$	$\dfrac{i_{L,peak}}{2} \cdot (d_1 + d_2)$

It is important to note that because the derivative of discontinuous state i_L in the third subinterval is zero, the corresponding entries of $\mathbf{A}_3$ and $\mathbf{B}_3$ have zeros too. Therefore, the correction coefficient ω_{31} could be any non-zero value which would multiply out with the corresponding column of $\mathbf{A}_3$ to zero and give the correct final result. Moreover, if the other two correction coefficients for the inductor current, ω_{11} and ω_{21}, are assumed to be equal, which holds if and only if

$$\frac{\bar{x}_1(1)}{d_1} = \frac{\bar{x}_2(1)}{d_2} \tag{24}$$

Then, one can easily set ω_{31} to be

$$\omega_{31} = \omega_{11} = \omega_{21} \tag{25}$$

So, if one assumes a triangular waveform of i_L and the condition (25), it can be readily verified that the correction matrix $\mathbf{M}$ as defined by (22) will come out diagonal with the entries exactly as those in [37], namely $\dfrac{1}{d_1 + d_2}$ and 1. However, in general, the correction coefficients (21) for the inductor current need not be equal and including parasitics of the circuit's components will violate (24) and (25). Consequently, the correction matrix $\mathbf{M}$ may be non-diagonal. The advantage of having a diagonal correction matrix is that each averaged state variable has its own

19

correction weight decoupled from the other states. Therefore, it is possible to define a modified correction matrix $\mathbf{M}_\Delta$ which can be made diagonal by construction. Specifically,

$$\mathbf{M}\overline{\mathbf{x}} = \mathbf{M}_\Delta \overline{\mathbf{x}} = \mathbf{p} \tag{26}$$

and

$$m_j = \mathbf{M}_\Delta(j, j) = \frac{\mathbf{p}(j)}{\overline{\mathbf{x}}(j)} \tag{27}$$

where $\mathbf{M}_\Delta$ is diagonal and m_j are its diagonal entries. Thereafter, $\mathbf{M}_\Delta$ is used in the corrected state-space averaged equation (23). Also, since the slow state variable v_C complies with the small ripple approximation, the entry of $\mathbf{M}_\Delta$ corresponding to slow state variable is usually around 1. In case of higher order converters, the correction matrix can be partitioned into a diagonal matrix for discontinuous state variables and identity matrix for continuous ones.

2.2.2 Analytical derivation of duty ratio constraint and the model order

In second-order dc-dc converters (i.e. boost, buck, and buck-boost) operating in discontinuous conduction mode, the transfer-functions exhibit dominant low frequency pole and zero due to the slow state variable dynamics. Pole and possible right-half-plan zero due to fast state variable dynamics are in higher frequencies near or exceeding switching frequency. To provide accurate average value model via space-state averaging, the second duty cycle known as the duty ratio constraint has been found to be the key point in difference between the full-order and the reduced-order models [37].

2.2.2.1   Reduced-order model

In discontinues conduction mode, fast state variable is clamped to a constant value in a prototypal switching cycle. As a result, the energy flowing in inductor is independent from cycle to cycle in a periodic waveform. From this point, one can argue that the fast state variable losses its meaning as state variable and can be removed from dynamic equations without significant effect. By neglecting dynamics of the fast state variable, the average value of $\overline{i}_L$, instead of differential equation may now be expressed as an algebraic function of the remaining systems variables (control signal d_1 and the average value of slow state variable $\overline{v}_C$) resulting in

reduced-order equations. Also, d_2 can be expressed as a function of the control signal d_1 and the average value of slow state variable $\bar{v}_C$ [33], [37], and [50].

Analytical derivation of reduced-order model is based on volt-second balance of the inductor over a prototypical switching interval. The ac voltage over inductor is assumed zero and dynamics of inductor current is neglected. From this perspective, as far as system behaviour is studied in frequencies significantly less than switching frequency (approximately, up to one tenth of switching frequency for phase study) the fast dynamics can be removed from system equations without significant effect. In higher frequencies, the errors especially in the phase plot of the bode diagram become very noticeable [37].

A procedure to extract the reduced-order models of any switch-mode converter based on the volt-second balance has been demonstrated in [50] and [67]. For example, the reduced-order models for ideal basic dc-dc converters in DCM are shown in Table 2.2 for consistency.

Table 2.2: Reduced-order models of basic dc-dc converters in DCM

Converter	Duty ratio constraint	Algebraic function of inductor current	Dynamic equation for capacitor voltage
Boost	$d_2 = \dfrac{v_g}{\bar{v}_C - v_g} \cdot d_1$	$\bar{i}_L = \dfrac{v_g}{2L} \cdot \dfrac{d_1^2 v_C T_s}{\bar{v}_C - v_g}$	$\dfrac{d\bar{v}_C}{dt} = \dfrac{v_{in}^2}{2LC} \cdot \dfrac{d_1^2 T_s}{\bar{v}_C - v_g} - \dfrac{\bar{v}_C}{RC}$
Buck	$d_2 = \dfrac{v_g - \bar{v}_C}{\bar{v}_C} \cdot d_1$	$\bar{i}_L = \dfrac{(v_g - \bar{v}_C)d_1^2 v_g T_s}{2L\bar{v}_C}$	$\dfrac{d\bar{v}_C}{dt} = \dfrac{d_1 v_g \bar{i}_L}{C\bar{v}_C} - \dfrac{\bar{v}_C}{RC}$
Buck boost	$d_2 = \dfrac{-v_g \cdot d_1}{\bar{v}_C}$	$\bar{i}_L = \dfrac{v_g}{2L} \cdot d_1^2 \cdot T_s(\dfrac{\bar{v}_C - v_g}{\bar{v}_C})$	$\dfrac{d\bar{v}_C}{dt} = \dfrac{v_g}{d_1 C} \cdot \dfrac{\bar{i}_L}{\bar{v}_C - v_g} - \dfrac{\bar{v}_C}{RC}$

A symbolic analysis program has been introduced to generate reduced-order averaged model from the net list of circuit under study [67]. The complexity of algebra involved in this frame work increases with complexity of system under study. Although the symbolic partitioned averaging in [67] and [68] address this issue for higher order converter, it also has several disadvantages; In particular, the amount of knowledge required by analyst to properly identify all the switching configuration, boundary conditions, fast and slow variables identification; and initial steady state conditions for fast variables, etc. is very significant.

Also, the slow-fast variable approach is not always applicable and, neglecting low frequency component in the fast state variable may lead to significant errors. For example, in a synchronous machine/rectifier system, the output voltage of rectifier is a fast state variable. This voltage has a high-frequency ripple component which doesn't affect the slow dynamics of system. However, during transient this voltage contains a low-frequency component that will affect the slow system [83]. Disadvantages of the reduced-order models may also limit their application in control design, especially where the fast state variable is to be observed and/or regulated (i.e. current mode control).

2.2.2.2 Full-order model

Although a discontinuous inductor current doesn't act as a state variable at low frequency, within each switching interval, it still has some average dynamic behaviour. In order to obtain a full-order state-space averaged model and capture the high frequency dynamics of inductor current i_L, the duty ratio constraint d_2 was represented in terms of the control signal d_1, the fast state variable $\bar{i}_L$ and the slow state variable $\bar{v}_C$, specially equivalent duty ratio [34], averaged switch modeling [36], loss free resistor [33, Chapter11]. There, the derivations of resulted full-order average value models are based on volt-second balance.

Since the inductor current starts from zero, and it returns to zero in each switching period, the average inductor voltage, computed over this period is indeed equal to zero. However, when considering a time varying source, the inductor dynamics implies that the voltage across the inductor may not always be zero. The average value of the inductor voltage over a prototypical switching interval may be computed by a so-called one switching cycle averaging (OSCA)[84]:

$$\bar{v}_L(kT_s + \tau) = \frac{1}{T_s} \int\limits_{(k-1)T_s+\tau}^{kT_s+\tau} v_L(\lambda)d\lambda \tag{28}$$

The output of (28) depends on the phase delay (represented by τ) between the starting of the switching interval and the start of integration. Particularly, the volt-second balance is true only if the phase shift τ is zero. This "averaging paradox" has been discussed, where it was clearly shown in time- as well as frequency-domain that OSCA is a sampling process of the true averaging. It was concluded that OSCA may result in modeling errors due to the violations of the

Nyquist sampling theorem [84]. Because the resulted high frequency pole in the transfer-function is not predicted accurately and consequently the phase-lag and magnitude drop caused by the inductor dynamics are over-estimated.

An accurate full-order average value model is represented in ([34], [35], [37], [48], [50], [69] and [70]) where the duty ratio constraint derivation is independent of volt-second balance. To describe the derivation of the duty ratio constraint for the new full-order model, the inductor current waveform of a lossless dc-dc converter in discontinuous conduction mode is shown in Fig. 2.2.
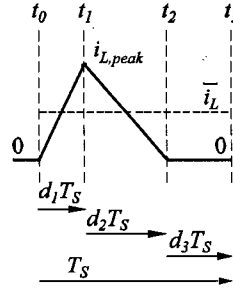

Fig. 2.2: Inductor current waveform in discontinuous conduction mode

As seen in Fig. 2.2, the inductor current increases linearly with time during the on-state of active switch and reaches its peak value at $t = d_1 T_s$.

$$
\begin{cases}
i_L(t) = \dfrac{V_{on}}{L} \cdot t & 0 < t < d_1 T_s \\
i_{L,peak} = \dfrac{V_{on}}{L} d_1 T_s
\end{cases}
\tag{29}
$$

After that, assuming resulted triangular wave shape, the average value of the inductor current is calculated using its peak.

$$
\bar{i}_L(t) = i_{L,peak} \frac{(d_1 + d_2)}{2}
\tag{30}
$$

Finally, by combining (29) and (30), a new duty ratio constraint for the full-order model is provided

$$
d_2 = \frac{2L\bar{i}_L}{d_1 T_s V_{on}} - d_1
\tag{31}
$$

Implementing the new definition of d_2 and previously obtained correction matrix $\mathbf{M}$ [37] in (8), the full-order models for lossless second-order dc-dc converters can be obtained. For consistency,

these models are summarized in Table 2.3, wherein the location of both low and high frequency poles and zeros are shown. For example, in boost converter, the second pole is located at $\frac{2(V_o/V_g - 1)f_s}{d_1}$ which can easily exceed the switching frequency. Also, possible right hand plan zeros are located at frequency $\frac{2f_s}{d_1}$ which is more than twice the switching frequency.

Table 2.3: Full-order state-space averaged models for basic dc-dc converters [35], [37], [50]

Converters	Averaged state-space equations	Low frequency pole	High frequency pole	RHP zero
Boost	$\dfrac{d\bar{i}_L}{dt} = \dfrac{2\bar{i}_L}{d_1 T_s}(1 - \dfrac{\bar{v}_C}{v_g}) + \dfrac{d_1 \bar{v}_C}{L}$ $\dfrac{d\bar{v}_C}{dt} = \dfrac{\bar{i}_L}{C} - \dfrac{d_1^2 T_s v_g}{2LC} - \dfrac{\bar{v}_C}{RC}$	$\dfrac{2\dfrac{V_o}{V_g} - 1}{(1 - \dfrac{V_o}{V_g})RC}$	$\dfrac{2(\dfrac{V_o}{V_g} - 1)f_s}{d_1}$	$\dfrac{2f_s}{d_1}$
Buck	$\dfrac{d\bar{i}_L}{dt} = \dfrac{d_1 v_g}{L} - \dfrac{2\bar{i}_L \bar{v}_C}{d_1 T_s(v_g - \bar{v}_C)}$ $\dfrac{d\bar{v}_C}{dt} = \dfrac{\bar{i}_L}{C} - \dfrac{\bar{v}_C}{RC}$	$\dfrac{2 - \dfrac{V_o}{V_g}}{(1 - \dfrac{V_o}{V_g})RC}$	$\dfrac{2\dfrac{V_o}{V_g}f_s}{d_1(1 - \dfrac{V_o}{V_g})}$	none
Buck-boost	$\dfrac{d\bar{i}_L}{dt} = \dfrac{d_1(v_g + \bar{v}_C)}{L} - \dfrac{2\bar{i}_L \bar{v}_C}{d_1 v_g T_s}$ $\dfrac{d\bar{v}_C}{dt} = \dfrac{\bar{i}_L}{C} - \dfrac{d_1^2 T_s v_g}{2LC} - \dfrac{\bar{v}_C}{RC}$	$\dfrac{2}{RC}$	$\dfrac{2\left|\dfrac{V_o}{V_g}\right|f_s}{d_1}$	$\dfrac{2f_s}{d_1}$

Most of the previous efforts in analytical average value model derivation are limited to ideal lossless topologies. Inaccuracies may occur as the result of parasitics in the circuit elements give rise to piece-wise non-linear current and voltage waveforms [85]. The generalization of analytical average value modeling to include ESR is limited to some specific converters [86]. Overall, the generalization of analytical derivation of state-space average value model of converters to include the ESR, nonlinearity, saturation, leakage, snubber, auxiliary circuit and other higher-order effects remains to be problematic and an open subject for research.

Analytical derivation of the duty ratio constraint in ideal converter assumes triangular waveshap of inductor current for the simplicity of derivation. Triangular waveshap implies constant voltage over inductor in each switching sub-instances. Although constant (or slowly varying) voltage source justifies this assumption for the first subinterval, the capacitor voltage dynamic is already neglected in second subinterval.

There are some switch-averaged models independent of converter operational mode [87]. However, the analytically derivation of the state-space averaged model is an operational mode-dependent process. The analytical derivation of d_2 in full-order state-space average value model is done assuming fast state variable $\bar{i}_L$ is in discontinuous conduction mode. The resulted state-space average value model is not functional if the converter operational mode changes to continuous conduction mode. The same discussion is valid for analytically derived state-space average value model in continuous conduction mode.

The analytical derivation of duty ratio constraint for lossless converters in discontinuous conduction mode is unique if the freewheeling current in the discontinuous subinterval d_3 is zero. In the case of other converters with multiple energy storage elements, the fast state variable might clamp to a nonzero constant value [24], [60]. The analytical derivation of the duty ratio constraint for converters with nonzero freewheeling current is different based on the converter under study.

If small ripple approximation is violated, the deviation of average value in (7) from true averaging maybe significant. In this thesis, it is suggested to compensate this difference in diagonal correction term $\mathbf{M}_\Delta$. In that case, the diagonal entry of the correction term matrix corresponding to continuous state variable may deviate from 1. The proposed numerical full-order state-space average value model is addressing all above mentioned discrepancies.

CHAPTER 3

Numerical Average Value Modeling

3.1 Model Construction

The detailed switching model (which includes all the necessary parasitics) is constructed first. If a state-variable approach is used to implement the detailed simulation, the system matrices $\mathbf{A}_k, \mathbf{B}_k, \mathbf{C}_k$ and $\mathbf{D}_k$ in each subinterval can be readily extracted numerically. Herein, without loss of generality, we assume that there is only one control input d_1 and one discontinuous conduction subinterval d_3. However, the methodology is extendable to converters with more complex topologies [17], [56], [88], [89]. In the detailed simulation, it is easier to extract correction matrix $\mathbf{M}_\Delta$ numerically instead of extracting the weighting correction matrices $\mathbf{W}_k$ in each subinterval. In the proposed framework, the diagonal elements of the correction matrix $\mathbf{M}_\Delta$ and the second duty cycle d_2 are obtained as functions of the duty cycle d_1 and the average value of the fast state variable $\bar{i}_L$, which results in a full-order model. Assuming that the system state-space matrices are available, the next step of constructing the required average value model consists of generating the functions of $d_2(d_1, \bar{i}_L)$ and $\mathbf{M}_\Delta(d_1, \bar{i}_L)$ numerically. To achieve that, the detailed model is run in the operating region of interest, whereas the state variables are averaged numerically over prototypical switching interval. In particular, the average value of state vector is computed in a steady state corresponding to a given operating point. Then, this value is inserted back into the state-space averaged equation (23) to find the overall correction matrix. Specifically, since in the steady-state $\dot{\bar{\mathbf{x}}} = 0$, we have

$$0 = \left(\sum_{k=1}^{3} d_k \mathbf{A}_k \right) \mathbf{M}_\Delta \bar{\mathbf{x}} + \left(\sum_{k=1}^{3} d_k \mathbf{B}_k \right) \mathbf{u} \tag{32}$$

from which the vector $\mathbf{p}$ is computed as

$$\mathbf{p} = -\left[\sum_{k=1}^{3} d_k \mathbf{A}_k\right]^{-1} \cdot \left[\sum_{k=1}^{3} d_k \mathbf{B}_k \mathbf{u}\right] \tag{33}$$

and the diagonal entries of $\mathbf{M}_\Delta$ are found using (27). To obtain $\mathbf{M}_\Delta(d_1, \bar{i}_L)$ and $d_2(d_1, \bar{i}_L)$ for the desired operating range the detailed simulation is run with different values of the control variable d_1 as well as the load r_{Load}. The variables resulted from this procedure are d_1, d_2, d_3, $\bar{i}_L$, and $\bar{v}_C$, whereas the correction matrix is computed using (27), (32) and (33). These variables are stored for the future use in lookup tables, wherein an interpolation/extrapolation may be used as necessary. A boost converter with parameters summarized in Appendix B.1 is considered here. The final numerical functions for m_1 and d_2 are plotted in Figs. 3.1 and 3.2, respectively. Since capacitor voltage is continuous, the m_2 entry is around 1 and is not plotted here. As expected, the obtained surfaces are continuous and smooth. It can be noted in Fig. 3.1 that m_1 is 1 in the region corresponding to continuous conduction mode. In discontinuous conduction mode, m_1 increases to compensate for the deficiency in conventional state-space averaging. In this mode m_1 becomes a nonlinear function of d_1 and $\bar{i}_L$. In Fig. 3.2, d_2 has a flat surface corresponding to continuous conduction mode and it varies linearly among the d_1-axis independent of $\bar{i}_L$ (as expected, $d_2 = 1 - d_1$). In discontinuous conduction mode, the surface of d_2 becomes non-linear and falls down abruptly.
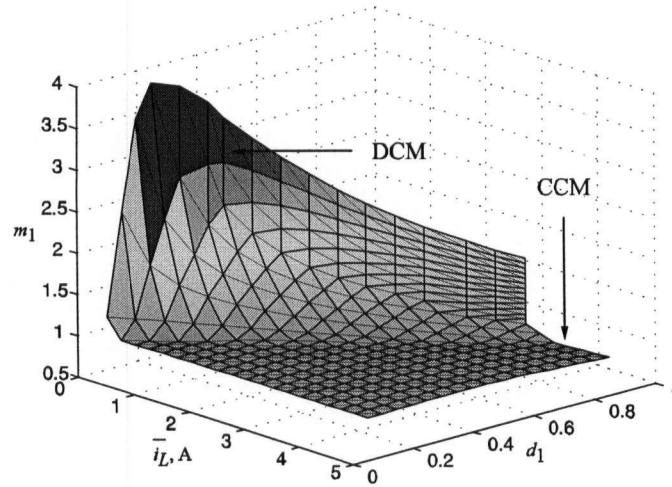

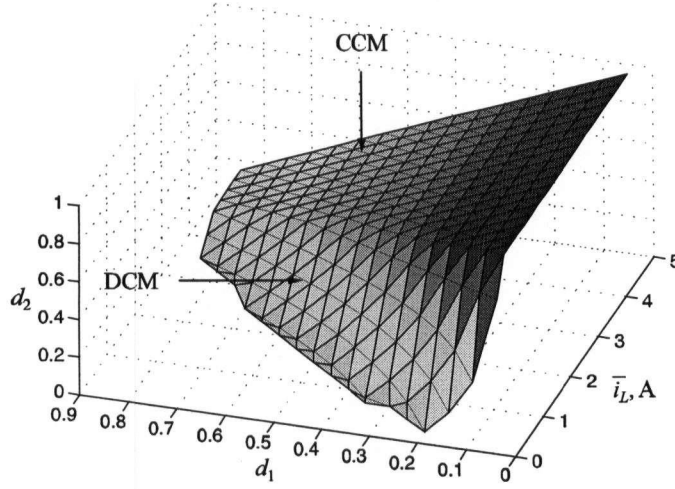Fig. 3.1: Fast state variable composite correction coefficient m_1

Fig. 3.2: Duty ratio constraint d_2

Once the functions $d_2(d_1, \bar{i}_L)$ and $\mathbf{M}_\Delta(d_1, \bar{i}_L)$ are available and stored, the proposed average value model is implemented according to the block diagram shown in Fig. 3.3. The system matrices for each subinterval are calculated numerically. For a given value of control variable d_1 and state vector $\bar{\mathbf{x}}$, the duty ratio constraint and correction term matrix are acquired through the lookup tables. Therefore, for a fixed input, the computed total averaged system matrices are state- and control-dependent.

$$
\begin{cases}
\mathbf{A}_T = \mathbf{A}_T(\bar{\mathbf{x}}, d_1) = [d_1\mathbf{A}_1 + d_2\mathbf{A}_2 + d_3\mathbf{A}_3]\mathbf{M}_\Delta \\
\mathbf{B}_T = \mathbf{B}_T(\bar{\mathbf{x}}, d_1) = [d_1\mathbf{B}_1 + d_2\mathbf{B}_2 + d_3\mathbf{B}_3] \\
\mathbf{C}_T = \mathbf{C}_T(\bar{\mathbf{x}}, d_1) = [d_1\mathbf{C}_1 + d_2\mathbf{C}_2 + d_3\mathbf{C}_3]\mathbf{M}_\Delta \\
\mathbf{D}_T = \mathbf{D}_T(\bar{\mathbf{x}}, d_1) = [d_1\mathbf{D}_1 + d_2\mathbf{D}_2 + d_3\mathbf{D}_3]
\end{cases}
\tag{34}
$$

These matrices are used to build a new continuous non-linear average value model which replaces the discontinuous detailed model.
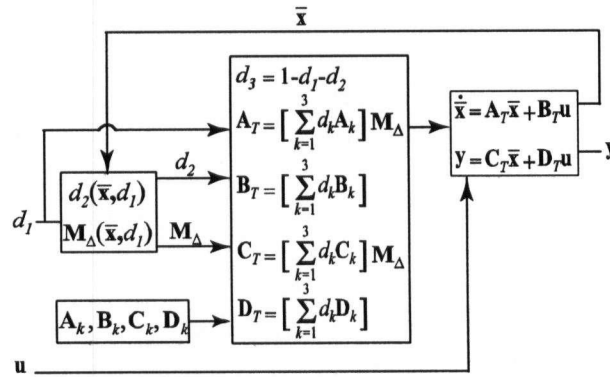

Fig. 3.3: Implementation diagram of the proposed average value model

28

3.2 Case Study of Boost Converter

The boost converter described in previous section is used as a benchmark in subsequent case studies. The converter parameters (including the parasitics) summarized in Appendix B.1 corresponding to the hardware prototype that has been built. The detailed model was implemented in Matlab/Simulink using the ASMG toolbox [90]. The ASMG code for this model is provided for consistency in Appendix C.1. The proposed numerical average value model has been compared with the hardware prototype, the detailed model, and the analytically derived average value model (Table 2.3) in time as well as frequency-domains.

3.2.1 Time-domain studies

The main parasitics of the hardware prototype have been included in the detailed model. The measured and simulated waveforms of the inductor current and the capacitor voltage corresponding to an operating point with $d_1 = 0.5$ and $r_{Load} = 15.12\Omega$ are shown in Figs. 3.4 and 8, respectively. The measured signals were filtered using a 3rd order Butterworth filter with 5MHz cut off frequency in order to reduce the noise in the measured signals. As it can be seen in Figs. 3.4 and 3.5, the detailed simulation matches the hardware measurement very well.
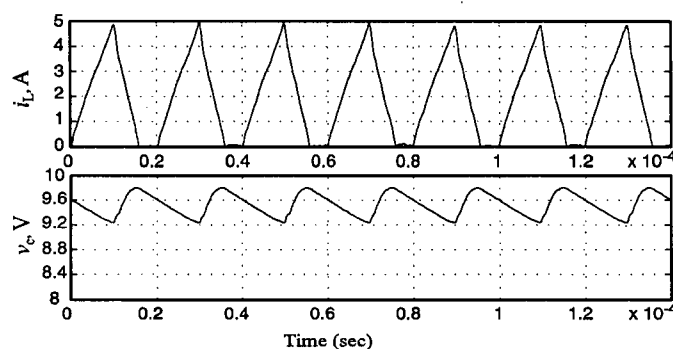
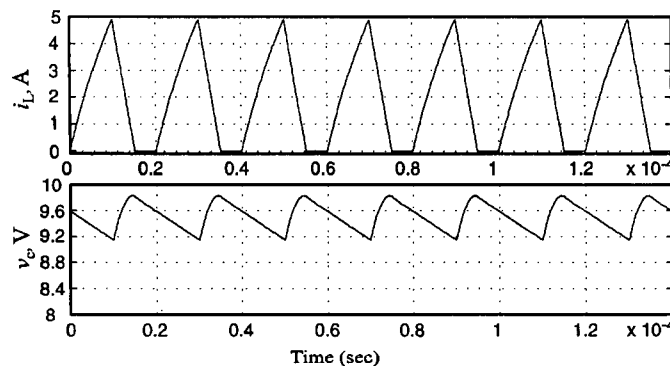Fig. 3.4: Measured inductor current and capacitor voltage

Fig. 3.5: Simulated inductor current and capacitor voltage

29

Since the proposed average value model has been extracted from the detailed model, it only approaches the detailed model in terms of accuracy. The accuracy of numerical average value model in predicting the large-signal behaviour in time-domain has been verified by studying the effect of sudden change in load. In the following study, the output of the boost converter was regulated utilizing a proportional-plus-integral (PI) controller as shown on a simplified diagram in Fig. 3.6. The PI controller was designed to regulate the output voltage at 15 volt by adjusting the duty cycle d_1. The controller parameters are $K_p = 0.1$ and $K_i = 50$.
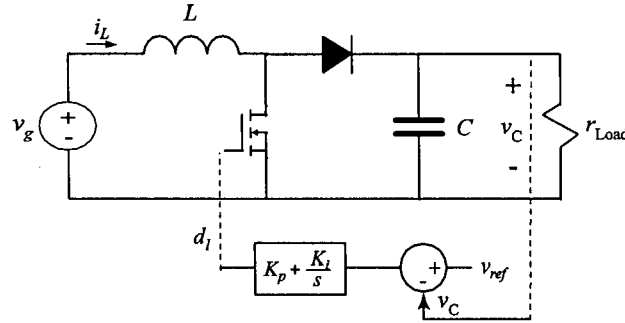

Fig. 3.6: Regulated boost converter

In the study considered, the converter initially operates in a steady state with a $40\,\Omega$ resistor attached to the output terminals. At $t = 0.0002$ sec., another $40\,\Omega$ resistor is connected in parallel to the load. The resulting time-domain transient is depicted in Fig. 3.7. As it can be seen in Fig. 3.7, first the inductor current is discontinuous and the converter operates in discontinuous conduction mode. After the step change in load, the output voltage has an initial dip and is recovering toward 15V, whereas the inductor current becomes continuous. Despite the change in operating mode, the numerical average value model predicts the overall transient envelope of the detailed system inductor current and capacitor voltage very well.
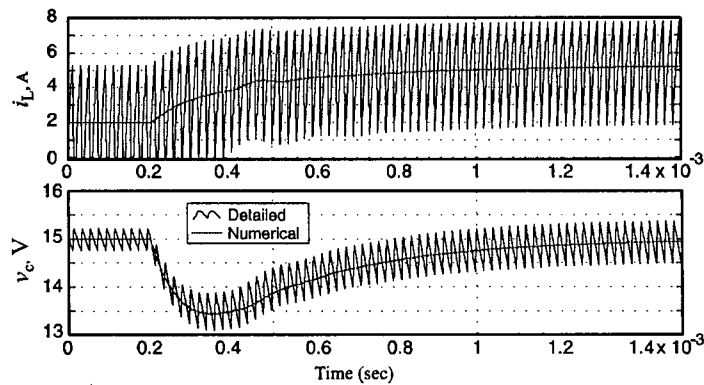

Fig. 3.7: Inductor current and capacitor voltage response to step change in load

In an ideal boost converter, the output voltage is always larger or equal to the input voltage. However, if parasitics are significant, the output voltage reduces and can even become less than the input voltage due to poor switch utilization. This phenomenon becomes especially pronounced when the duty cycle approaches unity, and as a result the conversion ratio decreases. Steady-state and small-signal analysis of switching circuit with parasitic have been studied in literature, for example [64], [91], and [92]. Parasitic effects are often considered in the design stage when the performance, efficiency and robustness of system are considered [93]. However, The advantage of the proposed numerical average value model is that essentially any parasitics included in the detailed model becomes automatically included in the generated average value model. To demonstrate this point, the following study is considered. The system initially operates in a steady-state with $r_{Load} = 5\Omega$ and $d_1 = 0.4$. At time $t = 0.0002$ sec., the duty cycle d_1 increases as a linear ramp function with the slop of 1000/sec from 0.4 to 0.95 which is reached at $t = 0.00075$ sec. As it can be seen in Fig. 3.8, the converter mode changes from discontinuous to continuous and finally the overloaded region of operation is reached. Throughout this entire study, the results predicted by the proposed numerical average value model remain in excellent agreement with the transient produced by detailed simulation.
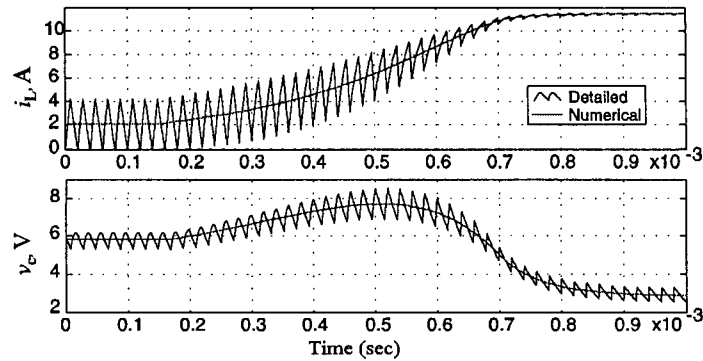

Fig. 3.8: Inductor current and capacitor voltage resulted from ramping the duty cycle

3.2.2 Frequency-domain studies

The small-signal control-to-output transfer-function ($\frac{\hat{v}_C(s)}{\hat{d}(s)}$) and the output-impedance transfer-function ($\frac{\hat{v}_C(s)}{\hat{i}_{Load}(s)}$) have been considered for verifying the proposed numerical average value model against the hardware prototype, the detailed simulation, and the analytically derived average value model. The small-signal injection and subsequent frequency sweep method has been implemented to extract the small-signal transfer-function from the hardware prototype and the detailed simulation corresponding to an operating condition of $r_{Load} = 15.12\Omega$ and $d_1 = 0.5$. The transfer-functions were evaluated up to 25 kHz which is a half of the switching frequency (50 *kHz*). Closer to the switching frequency the results become distorted due to interaction between the injected perturbations and the converter switching. In general, considering frequencies close to and above the switching frequency has limited use for the average model since the basic assumptions of averaging are no longer valid. Since the average value models are continuous, they have been linearized about the same operating point and respective transfer-functions were then readily extracted numerically using linear system's tools [Simulink LTI viewer].

The resulting control-to-output and output-impedance transfer-functions are plotted in Figs. 3.9 and 3.10, respectively. Since the numerically generated average value model only approaches the detailed simulation in terms of accuracy, the data points produced by the detailed model are considered herein as reference. As it can be seen in Fig. 3.9, the analytical average-value model differs from the hardware measurement and the detailed model especially in the magnitude of control-to-output transfer-function. This noticeable mismatch is attributed to the fact that the parasitics were not included in analytical derivations [37]. However, the development of the numerical average value model predicts the control-to-output transfer-function shown in Fig. 3.9 as well as the output impedance shown in Fig. 3.10 with an excellent agreement between the measured data and the results from the detailed simulation.
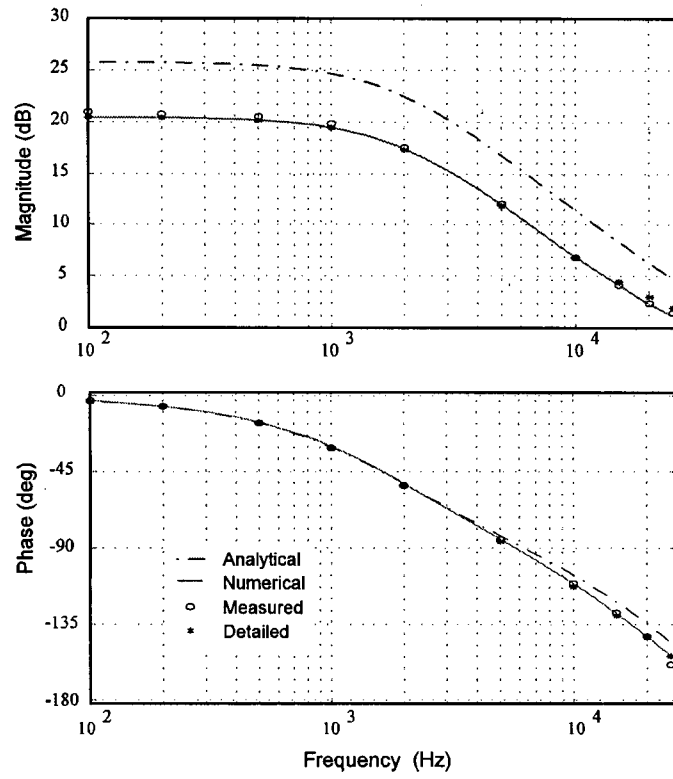
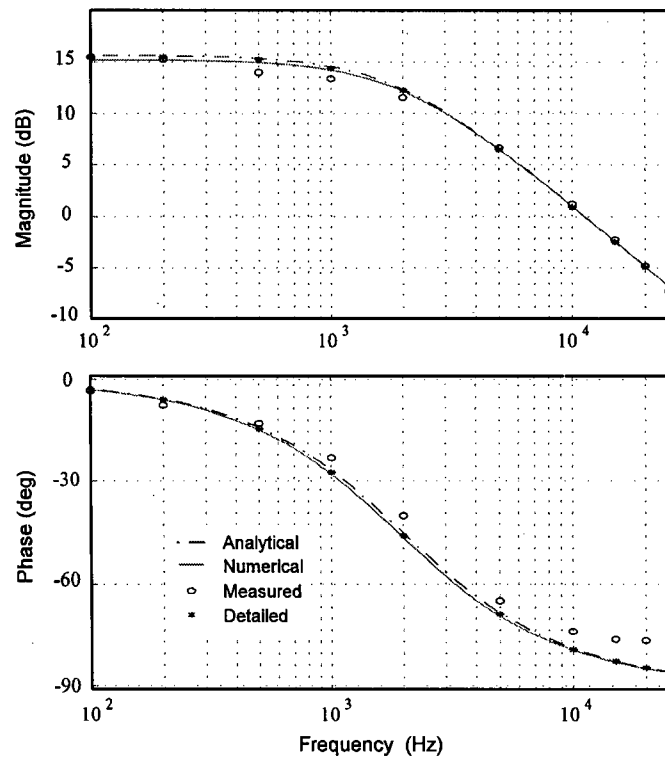Fig. 3.9: Control-to-output transfer-function

Fig. 3.10: Output-impedance transfer-function

33

CHAPTER 4

Generalized Parametric State-Space Average Value Modeling

4.1   Generalized Approach with Switching-Cell Dynamic Impedance

The output-impedance and control-to-output transfer-functions have been provided without the source dynamics. In particular, in the proposed average value model, values of the second duty cycle d_2 and the correction matrix $\mathbf{M}_\Delta$ were derived based on the average value of fast state variable $\bar{i}_L$ and active duty cycle d_1 with fixed v_g. Therefore, in the previously described approach with the established functions $d_2(d_1, \bar{i}_L)$ and $\mathbf{M}_\Delta(d_1, \bar{i}_L)$ the changes in the input voltage source and/or input impedance are not supported.

However, the input-to-output ($\dfrac{\hat{v}_C(s)}{\hat{v}_g(s)}$) and input-impedance ($\dfrac{\hat{v}_g(s)}{\hat{i}_g(s)}$) transfer-functions are of very significant interest and appear in control schemes and stability analysis, for example in [94]. The output impedance determination is a vital stage in the stability analysis of multi-converter cascaded or paralleled systems [27], [95], [96]. Moreover, in multi-converter systems, the voltage source v_g might be provided from a filtered output of an ac-dc rectifier or another cascaded converter. Such output will typically include ripple in addition to its dominant dc value. Also, there are converter topologies that utilize multiple input sources in hybrid energy systems [97]. However, the state-space averaged model developed in Chapter 3 was based on slowly varying source [see Eq. (6)].

In the final state-space average value model depicted in Fig. 3.3, the duty ratio constraint d_2 and correction matrix $\mathbf{M}_\Delta$ can be expressed as functions of state variables ($\bar{i}_L, \bar{v}_C$), control d_1 and

input v_g. For some specific topologies, such as basic second-order dc-dc converters, these functions are independent of the slow state variable. However, a more general approach is needed that would allow including the input source dynamics. Thus, in order to establish an average value model that is valid for input as well as output disturbances, it may be necessary to include the slow state variable as well as the input voltage as arguments for the functions d_2 and $\mathbf{M}_\Delta$. On one hand, a straightforward extension of this approach implies that the numerical functions of d_2 and $\mathbf{M}_\Delta$ should be defined in terms of a total of four arguments v_g, d_1, $\bar{i}_L$, and $\bar{v}_c$. On the other hand, it is desirable to re-combine these variables into the smallest possible number of inputs. For example, in order to capture the source perturbations, one might suggest lamping two variables into an impedance defined as $\dfrac{v_g}{\bar{i}_L}$. However, as it will be shown in Section 4.4 (case of Cuk converter), the slow state variable should also be included. Therefore, in the proposed approach, a so-called switching-cell dynamic impedance is defined as

$$z_{sw-cell} = \left| \frac{\bar{v}_g - \bar{v}_c}{\bar{i}_L} \right| \tag{35}$$

Which combines three of the mentioned variables in a compact and meaningful way. Thereafter, the diagonal elements of correction matrix $\mathbf{M}_\Delta$ and the duty ratio constraint d_2 are obtained as functions of the duty cycle d_1 and the switching-cell dynamic impedance $z_{sw-cell}$. Assuming that the system state-space matrices are available, the next step of constructing the required average value model consists of generating the functions of $d_2(d_1, z_{sw-cell})$ and $\mathbf{M}_\Delta(d_1, z_{sw-cell})$ numerically. The process of obtaining these functions is similar to the one described in Chapter 3. The final numerical functions for m_1 and d_2 for basic dc-dc converters are plotted in Figs. 4.1-4.6, respectively. Since the capacitor voltage is continuous and the small ripple approximation holds, the m_2 entries are around 1 and are not plotted here. The corresponding parameters of boost, buck, and buck/boost are summarized in Appendices B. 1-3, respectively.

The obtained composite correction term m_1 and duty ratio constraint d_2 for the basic dc-dc converters may be interpreted, similar to the discussion in Chapter 3. As expected, the obtained surfaces are continuous and smooth. In all cases, m_1 is 1 in the region corresponding to
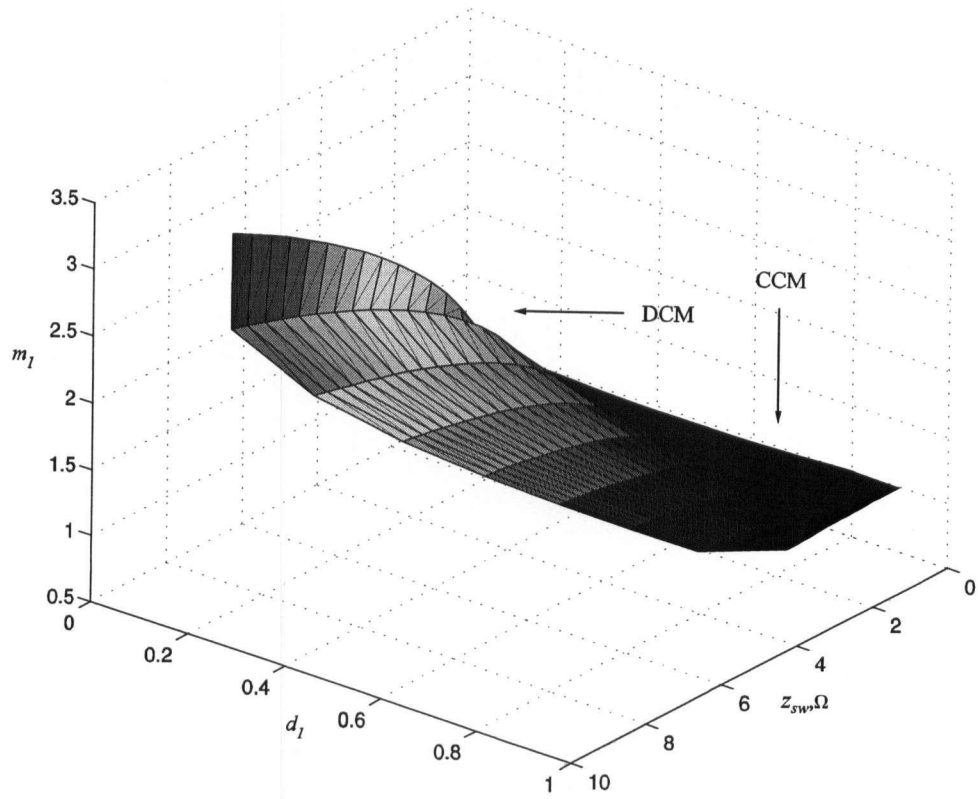
Fig. 4.1: $z_{sw-cell}$ composite correction coefficient m_1 for boost converter model
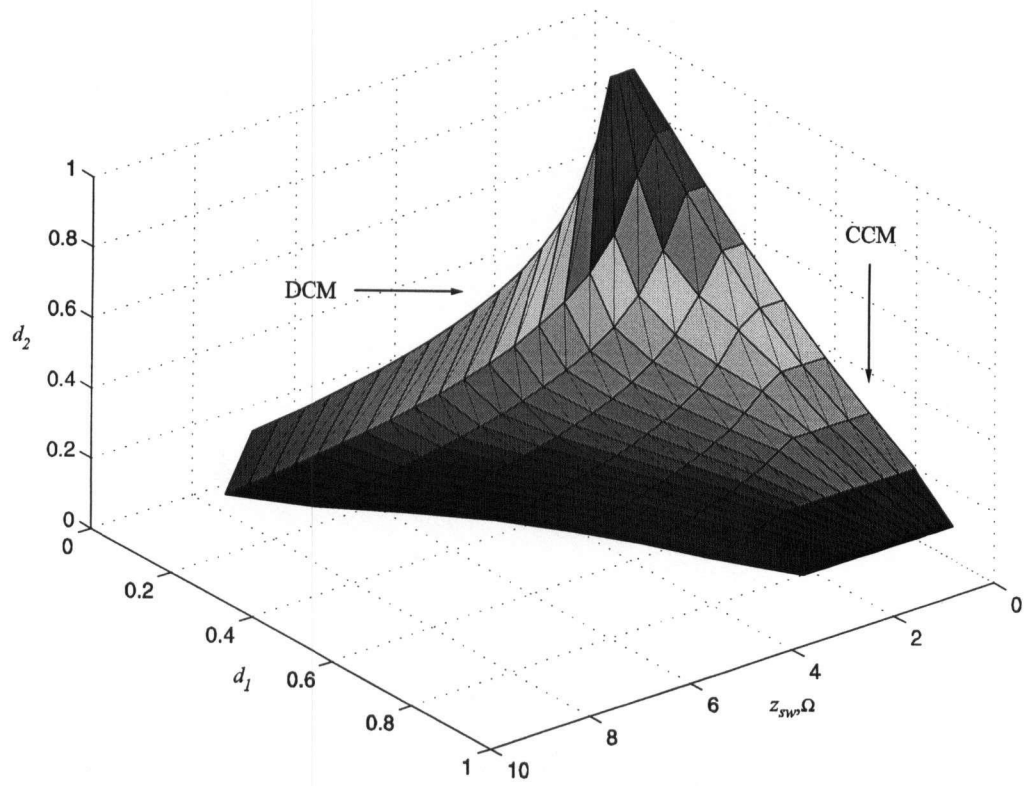

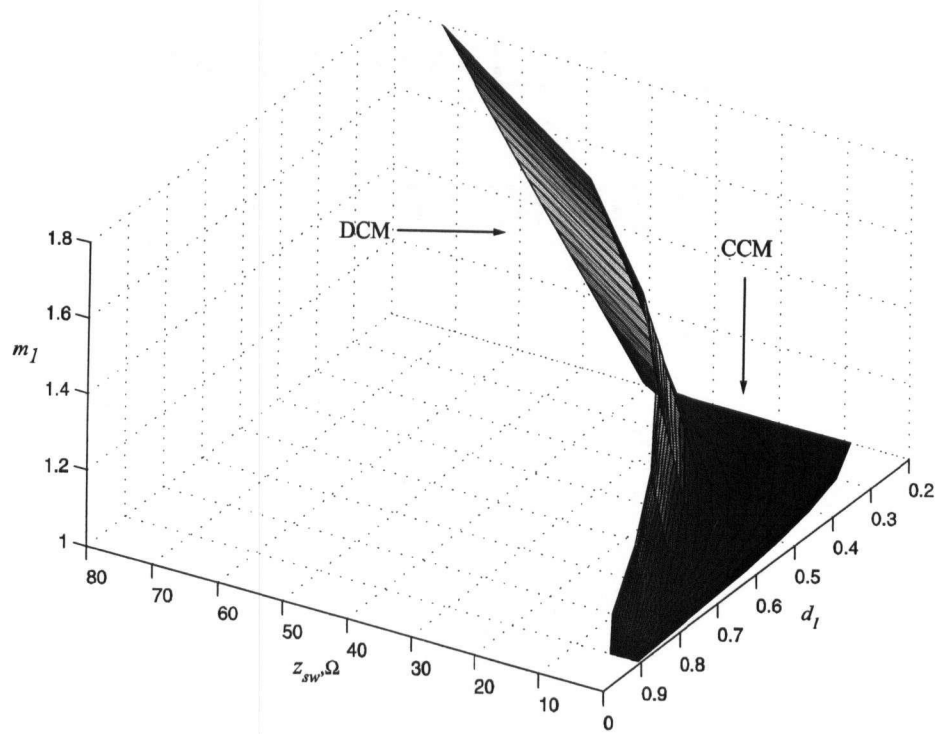Fig. 4.2: Duty ratio constraint d_2 for boost converter model

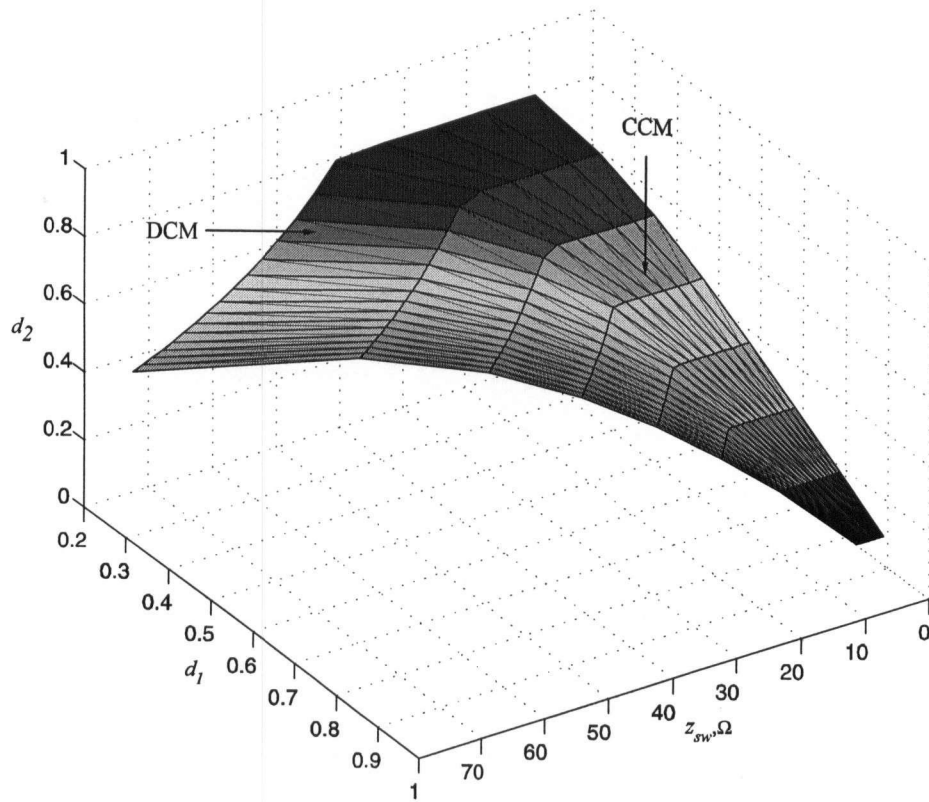Fig. 4.3: $z_{sw-cell}$ composite correction coefficient m_1 for buck converter model

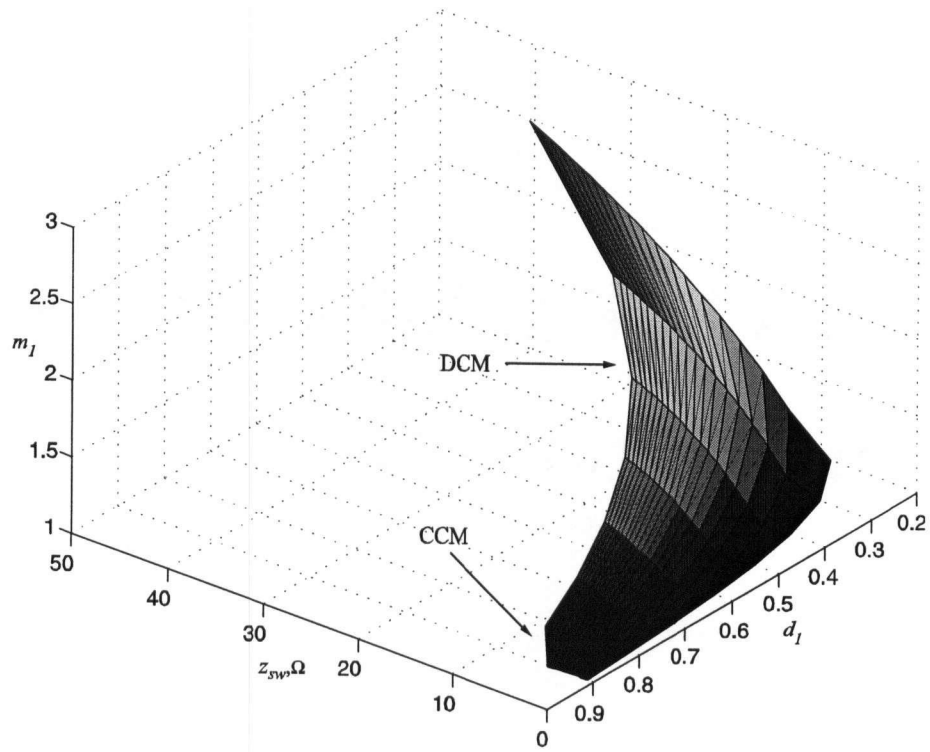Fig. 4.4: Duty ratio constraint d_2 for buck converter model

Fig. 4.5: $z_{sw-cell}$ composite correction coefficient m_1 for buck/boost converter model
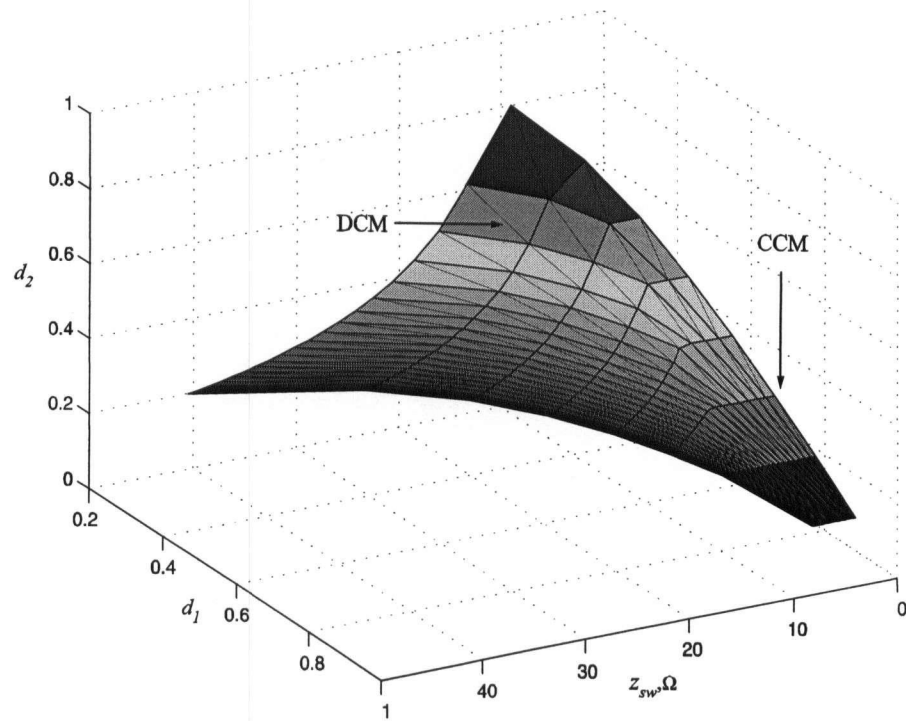

Fig. 4.6: Duty ratio constraint d_2 for buck/boost converter model

4.2 Computer Aided Small-Signal Characterization of Switching Converters

Conventional frequency-domain characterization methods are approximated and/or computationally intensive. Although proposed generalized numerical average value modeling predicts small-signal transfer-functions accurately, it is not required to run the simulation over a large operation range for local small-signal characterization. Herein, a fast computer-aided frequency-domain characterization scheme via the proposed generalized numerical average value modeling is introduced:

1. Given the loading/operating conditions, the detailed switching dc-dc converter is run with small perturbations in duty cycle and switching-cell dynamic-impedance $z_{sw-cell}$ values.

2. The average values of state $\bar{x}$ in steady state are saved for the perturbed points. The switching-cell dynamic-impedance $z_{sw-cell}$ and the diagonal correction term matrix $\mathbf{M}_\Delta$ are calculated using (27), (32), (33), and (35). The numerical functions of $\mathbf{M}_\Delta \left(d_1, z_{sw-cell} \right)$ and $d_2 \left(d_1, z_{sw-cell} \right)$ corresponding to the operating point of interest are stored as small data sets.

3. Finally, with provided data sets, an implementation similar to generalized average value modeling yields a nonlinear continuous model. This model is then numerically linearized to provide the small-signal characterization around the specified operating point.

4.3   Basic PWM DC-DC Converters Case Studies

The generalized parametric state-space average value modeling is implemented on the three basic PWM dc-dc converters; buck, boost, and buck/Boost. The large-signal transient of the proposed model has been compared with detailed switching simulation in time-domain. All benchmarks include time-varying input sources. Also input-to-output transfer-function is included in frequency-domain studies. The time-domain transient study involves both continuous and discontinuous conduction modes. The small-signal transfer-functions of the proposed numerical models have been compared with the analytically averaged and the detailed switching simulations.

4.3.1 Boost converter

A buck-fed boost converter shown in Fig. 4.8 is used as a benchmark. The output of the buck converter is considered as input v_g for the boost converter. This system assembles a non-inverting cascaded Buck/Boost converter. The value for C_1 is chosen for dynamic stability [96] as well as dc bus ripple control. The main parasitics of this two-converter system have been included in the detailed switching model. For consistency, the system parameters are summarized in Appendix B.4. Also, the corresponding ASMG codes for the buck and the boost converters are provided in Appendix C. 2 and Appendix C. 1, respectively.
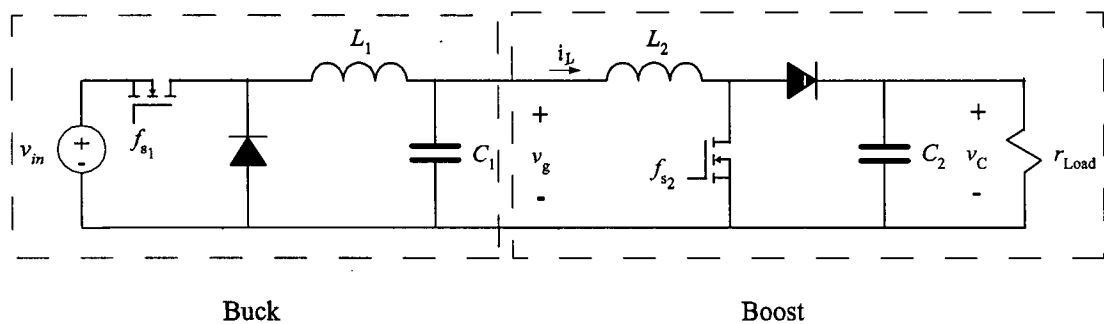

Fig. 4.8: Boost converter fed by buck converter

The accuracy of the numerical average value model in predicting the large-signal in time-domain behaviour of the boost converter has been verified by studying the sudden change in load. In the

study considered here, the converter initially operates in a steady-state with a 40 Ω resistor attached to the output terminals. At $t = 0.0005$ sec., another 4.4 Ω resistor is connected in parallel to the load. The resulting time-domain transient is depicted in Fig. 4.9. As it can be seen in Fig. 4.9, the inductor current is first discontinuous and the boost converter operates in DCM. After the step change in load, the boost converter goes to CCM. The buck converter is in DCM throughout the study and its output voltage is load-dependent. The slow variation in dc voltage v_g is due to buck converter switching, while the fast ripple v_g is due to the boost converter switching, both highlighting the time varying characteristic of input voltage for the boost converter. Despite the change in operating mode and variation in input voltage, the numerical average value model predicts the overall transient envelope of the detailed system inductor current and capacitor voltage very well.
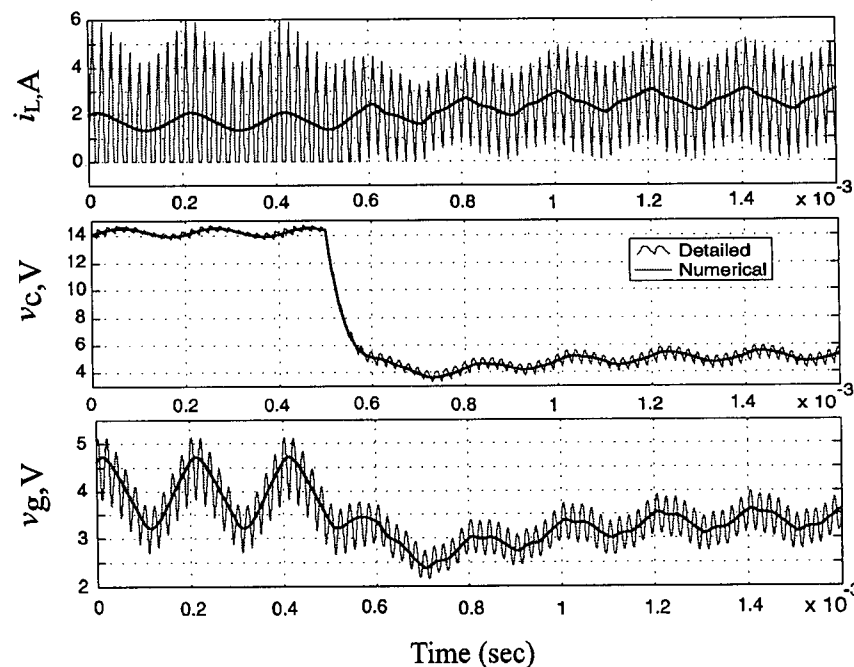
Fig. 4.9: Boost inductor current, capacitor voltage, and input voltage (buck output voltage) responses to step change in load

The small-signal input-to-output transfer-function and the output-impedance transfer-function have been considered for verifying the proposed numerical average value model against the detailed simulation and analytical average value model. To extract the small-signal transfer-functions of the boost converter, the buck converter has been replaced with a constant voltage source $v_g = 4V$. The small-signal injection and subsequent frequency sweep method has been

42

implemented to extract the transfer-function from the detailed simulation. The boost converter operates in discontinuous conduction mode with $r_{Load} = 15.12\Omega$ and $d_1 = 0.5$. The transfer-functions are evaluated up to 25 kHz which is a half of the boost converter switching frequency (50 kHz). Since the average value models are continuous, they have been linearized about the same operating point and respective transfer-functions were then readily extracted.

The resulting input-to-output and output-impedance transfer-functions are plotted in Figs. 4.10 and 4.11, respectively. As it can be seen, especially in the magnitude plot of Fig. 4.10, the analytical average value model results differ from the detailed model ones. This noticeable mismatch is mainly attributed to the parasitic effects as well as inaccurate prediction of operating point corresponding to a specific loading condition. However, the developed numerical average value model predicts the input-to-output transfer-function shown in Fig. 4.10 as well as the output impedance shown in Fig. 4.11 with an excellent agreement with the detailed simulation.
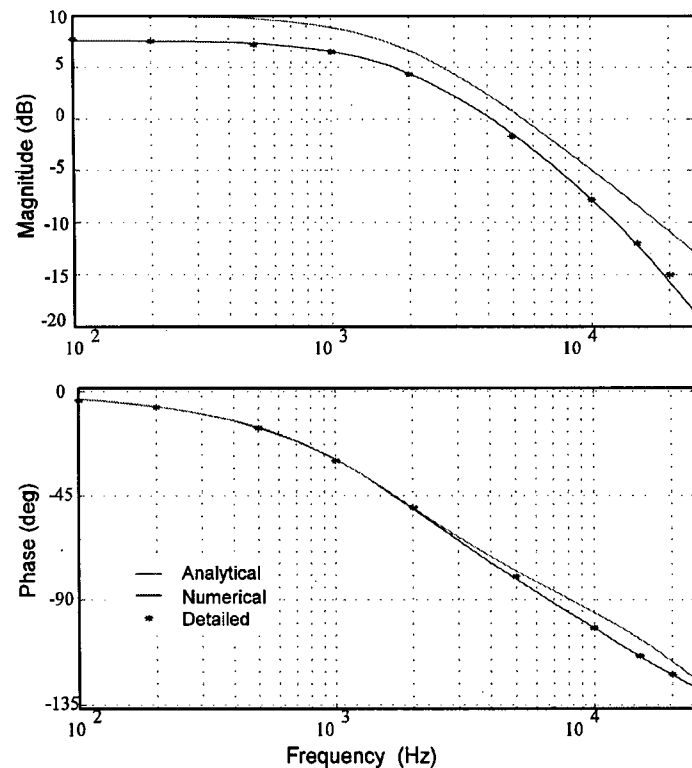

Fig. 4.10: Boost converter input-to-output transfer-function
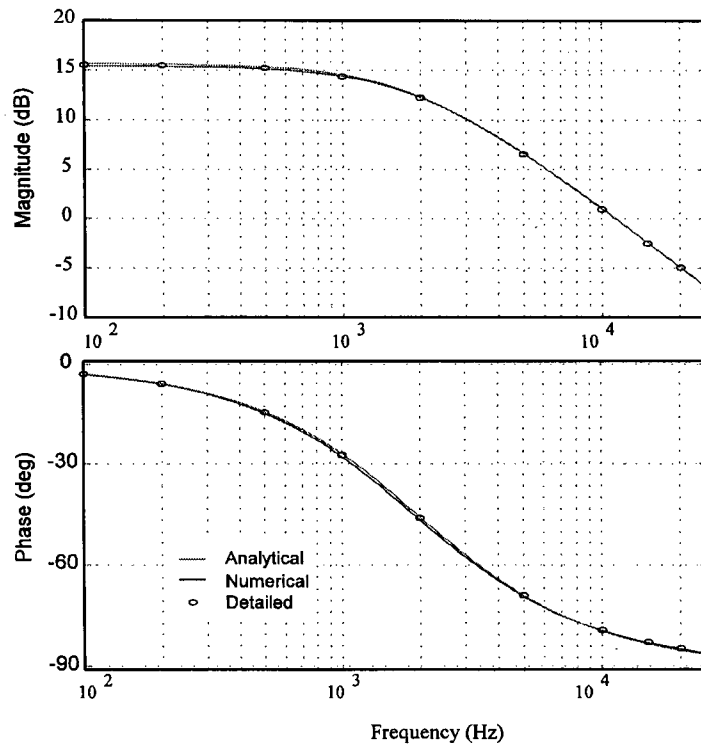
Fig. 4.11: Boost converter output-impedance

4.3.2 Buck converter

A rectifier-fed buck converter shown in Fig. 4.12 is used as a benchmark here. A single-phase ac voltage source is rectified using a single-phase H-bridge. The rectified voltage is filtered using a low-pass filter composed of L_f and C_f. The capacitor voltage of the low pas filter is used as an input voltage v_g for the buck converter. The main parasitics of the rectifier-fed converter system have been included in the detailed switching model. For consistency, the system parameters are summarized at Appendix B.5. Also, the corresponding ASMG codes for the rectifier and the buck converters are provided in Appendix C. 3 and Appendix C. 4, respectively.
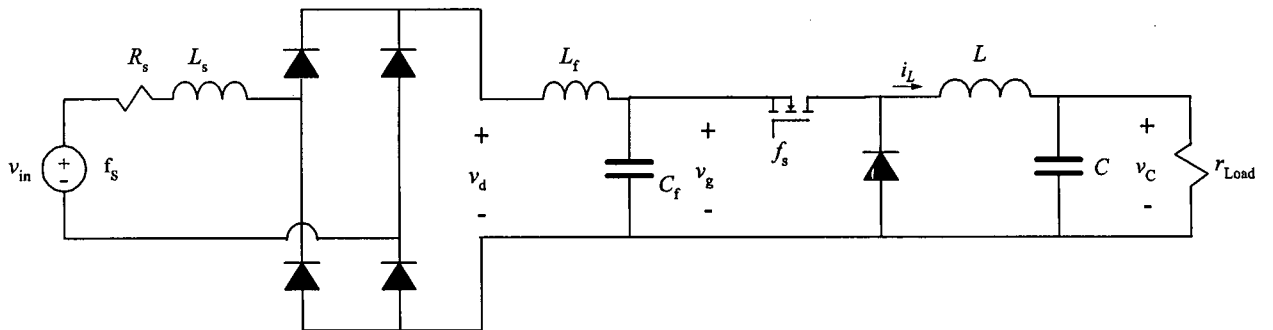
Fig. 4.12: Rectifier-fed buck converter circuit diagram

44

The system starts up in DCM with initial conditions corresponding to a steady-state operation with $d_1 = 0.5$ and a load resistance of $20\,\Omega$. At $t = 0.0004$ sec., another $5\,\Omega$ resistor is connected in parallel to the load. The resulting time-domain transient is depicted in Fig. 4.13, wherein the buck converter mode changes from DCM to CCM. The slow variation in the voltage v_g is twice the ac source frequency ($f_s = 5\,\text{kHz}$), while the fast variation is due to the boost converter switching. Despite the variation in the source voltage, the numerical averaged model is able to predict the transition from CCM to DCM with excellent accuracy.
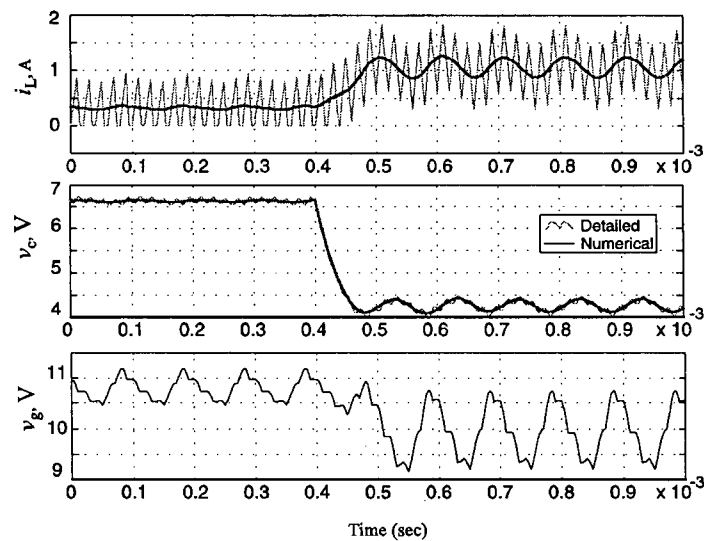
Fig. 4.13: Buck inductor current, capacitor voltage, and input voltage source (rectifier output voltage) responses to step change in load

The input-to-output and the output-impedance transfer-functions are considered for verification of the proposed numerical average value model in frequency-domain. To exclude the switching effects of the H-bridge on resulted transfer-functions, the filtered rectifier has been replaced with a constant source voltage $v_g = 12V$. The resulting input-to-output and output impedance transfer-functions are plotted in Figs. 4.14 and 4.15, respectively. The buck converter operates in discontinuous conduction mode with $r_{Load} = 20\Omega$ and $d_1 = 0.5$.
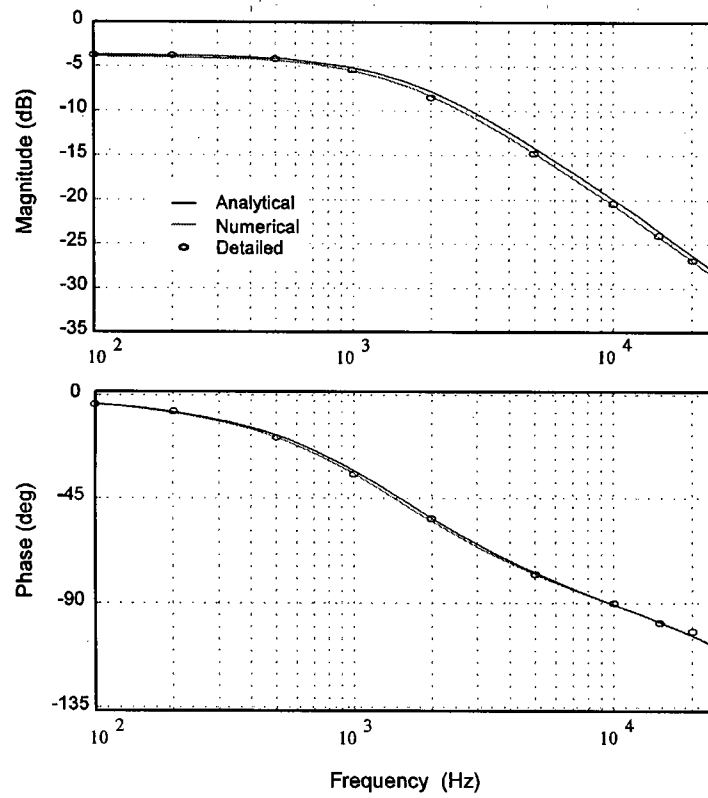
Fig. 4.14 : Boost converter input-to-output transfer-function
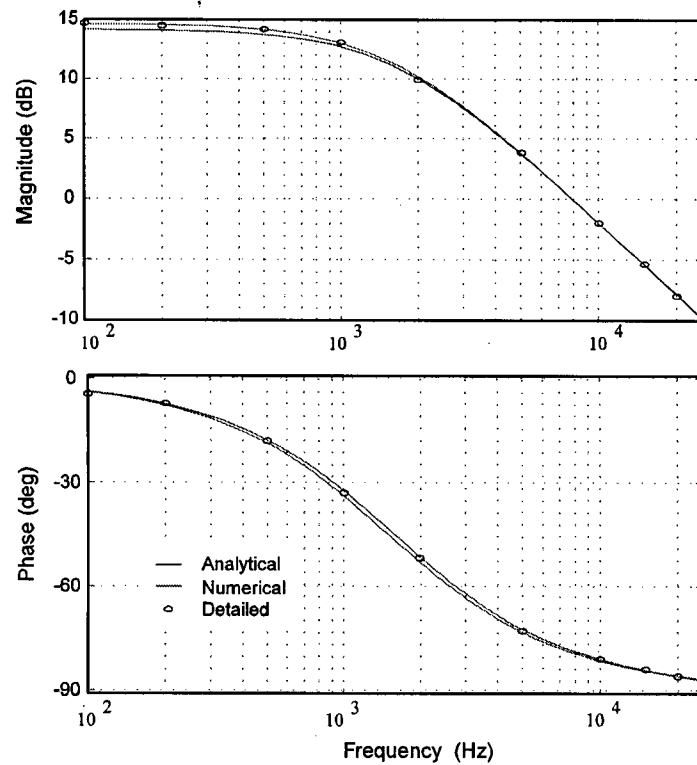
Fig. 4.15: Buck converter output-impedance transfer-function

4.3.3 Buck/boost converter

A variable source buck/boost converter shown in Fig. 4.16 is used as a benchmark here. The main parasitics of the buck/boost converter system have been included in the detailed switching model. The switching frequency is adjusted to $f_s = 100kHz$. For consistency, the system parameters are summarized in Appendix B.3. Also, the corresponding ASMG codes for the buck/boost converter are provided in Appendix C. 5.
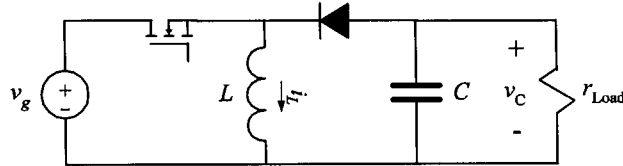
Fig. 4.16: Buck/boost converter

In the computer study considered, the system starts up in CCM with initial conditions corresponding to a steady-state operation with $d_1 = 0.5$, $v_g = 5V$, and a load resistance of 4Ω. At $t = 0.0002$ sec., the load resistor is increased to 50Ω, and the inductor current becomes discontinuous. After that, at $t = 0.0004$ sec. the input voltage source is step changed to $v_g = 10V$, resulting in a large-signal transient depicted in Fig. 4.17. As it is shown in Fig. 4.17, the responses of Numerical model follow almost exactly the traces produced by detailed model during entire study.
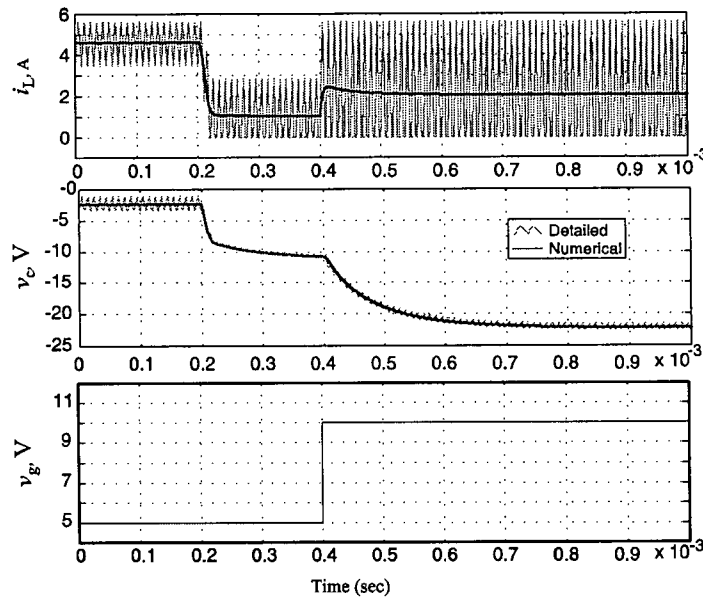

Fig. 4.17: Buck/boost inductor current, capacitor voltage, and input voltage source responses to step change in load followed by the sudden change in input voltage

47

Similar to previous converters, the proposed model is also verified in frequency-domain by considering the small-signal input-to-output and output-impedance transfer-functions. The transfer function are extracted in a steady-state corresponding to an operating condition determined by $r_{Load} = 10\Omega$, $d_1 = 0.5$, and $v_g = 5V$. The resulting input-to-output and output-impedance transfer-functions are evaluated up to 50 kHz and plotted in Figs. 4.18 and 4.19, respectively. As it can be seen here, the analytically derived model matches the detailed model in low frequency and deviates in higher frequencies. At the same time, the proposed numerical average value model predicts almost identical results as the detailed simulation throughout the entire frequency range.
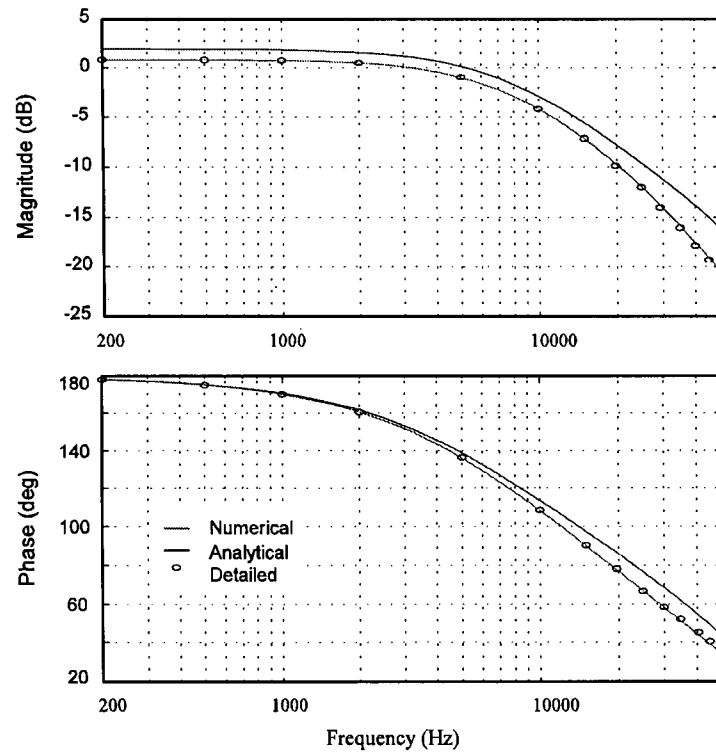
Fig. 4.18: Buck/boost input-to-output transfer-function

f
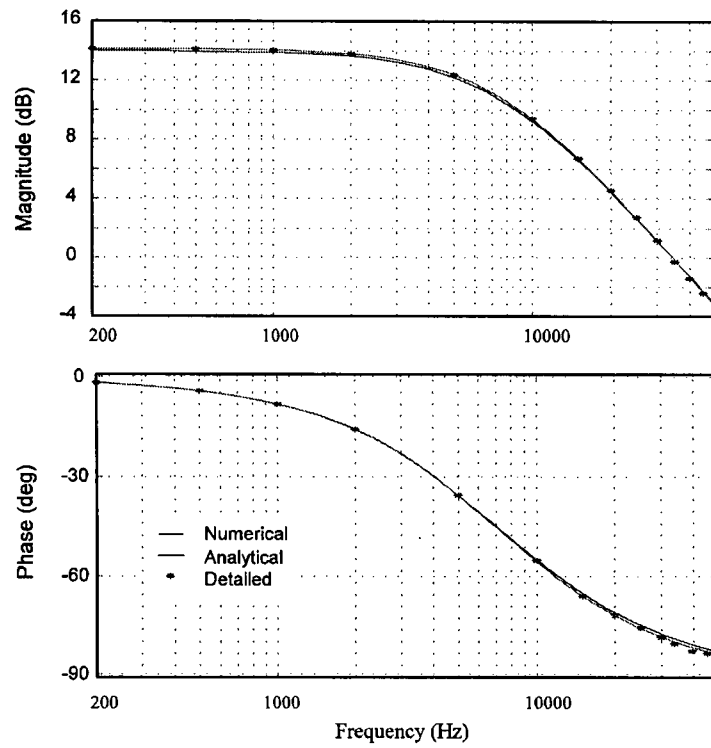
Fig. 4.19: Buck/boost converter output-impedance transfer-function

4.4 Discontinuous Conduction Mode in Cuk Converter
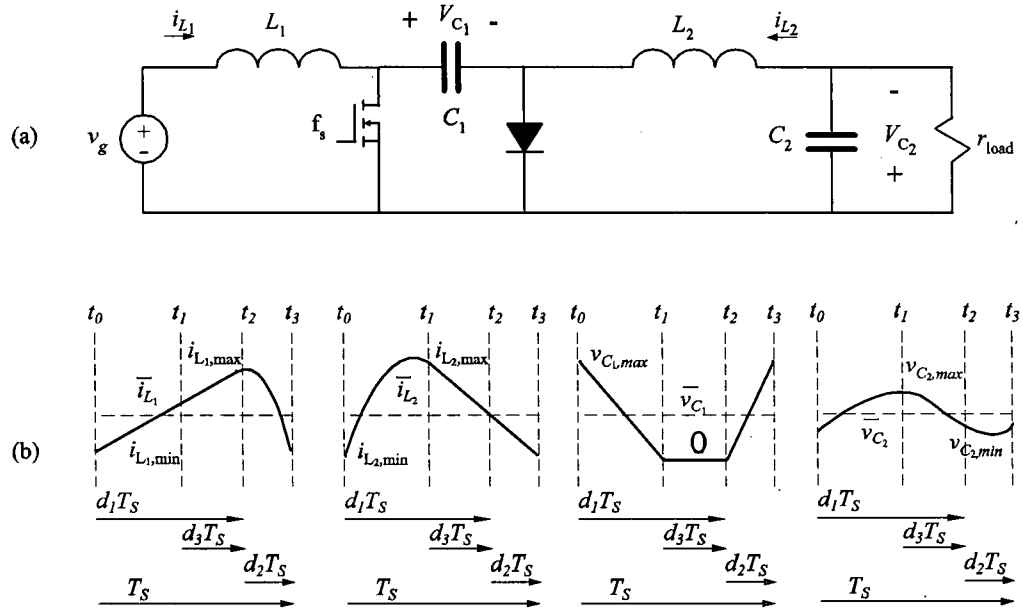
Fig. 4.20: (a) Cuk converter circuit diagram; (b) state variables waveforms in DCM

There are numerous motivations to seek an average value model for cuk converter, where applicable analytical average value models are not readily available. The proposed methodology has been already shown to work well for the second-order dc-dc converters. This general methodology is easily extendible for the higher order converters, where the correction matrix is partitioned into an identity sub-matrix for the continuous state variables and a diagonal correction sub-matrix for the discontinuous state variables. In higher order converters, the discontinuity might happen for individual state variables as well as their linear combination. For example in the Cuk converter shown in Fig. 4.20, two different discontinuous conduction modes are common:

1) $i_{L_1} + i_{L_2}$ is discontinuous (DICM)

2) v_{C_1} is discontinuous (DCVM)

Since the capacitor C_1 suffers current ripples of both i_{L_1} and i_{L_2}, the capacitor voltage discontinuity is frequently encountered, especially when the capacitor C_1 is small. Therefore, DCVM, as the dual case of DICM, is of special concern for investigation.

4.4.1 Extension of generalized parametric averaging to the cuk converter

The proposed general parametric state-space average value modeling based on switching-cell dynamic-impedance has been validated for discontinuous inductor current mode. The inductor current is chopped to zero when both switches in the switching cell are disconnected. In the dual case of capacitor voltage discontinuity, there is an interval when both switches in the voltage loop with the capacitor C_1 are connected simultaneously. Since the active switch on-state is directly controlled by d_1, the discontinuity subinterval d_3 is already included in d_1. The proposed methodology is general and easily extendible to discontinuous capacitor voltage mode with slight modification in the switching-cell dynamic-impedance definition and model implementation based on the converter under study.

In underlying Cuk converter, the switching cell is composed of the active switch, the capacitor C_1, and the diode. The voltage over the switching-cell is v_{C_1}, and the current entering switching-cell network is $i_{L_1} + i_{L_2}$. Therefore, the switching-cell dynamic impedance is defined as:

$$z_{sw-cell} = \frac{\bar{v}_{C_1}}{\bar{i}_{L_1} + \bar{i}_{L_2}} \tag{37}$$

Aassuming that the state-space matrices are available, the next step of constructing the required average value model consists of generating the functions of $d_3(d_1, z_{sw-cell})$ and $\mathbf{M}_\Delta(d_1, z_{sw-cell})$ numerically. The process is the same as in discontinuous inductor current case described before. The generated numerical functions are shown in Figs. 4.21 and 4.22 for the cuk converter with parameters summarized in Appendix B.6.

Since the capacitor voltage v_{C_2}, the inductor current i_{L_1}, and the inductor current i_{L_2} are continuous and the small ripple approximation holds, m_1, m_2, and m_4 entries are around 1 and are not plotted here. In Fig. 4.21, the discontinuous subinterval d_3 corresponding to continuous conduction mode is zero and independent of d_1 and $z_{sw-cell}$. In discontinuous conduction mode, d_3 is not zero anymore and increases as nonlinear function of d_1 and

51

$z_{sw-cell}$. Here d_2 is simply a linear function $d_2 = 1 - d_1$ and is not plotted. It can be noted in Fig. 4.22 that m_3 is 1 in the region corresponding to continuous conduction mode. In discontinuous conduction mode, m_3 increases to compensate for the deficiency in conventional state-space averaging. In this mode, m_3 becomes a nonlinear function of d_1 and $z_{sw-cell}$.

Once the functions $d_3(d_1, z_{sw-cell})$ and $\mathbf{M}_\Delta(d_1, z_{sw-cell})$ are available and stored, the proposed average value model is implemented according to the block diagram shown in Fig. 4.7 with appropriate modification for d_3 instead of d_2.
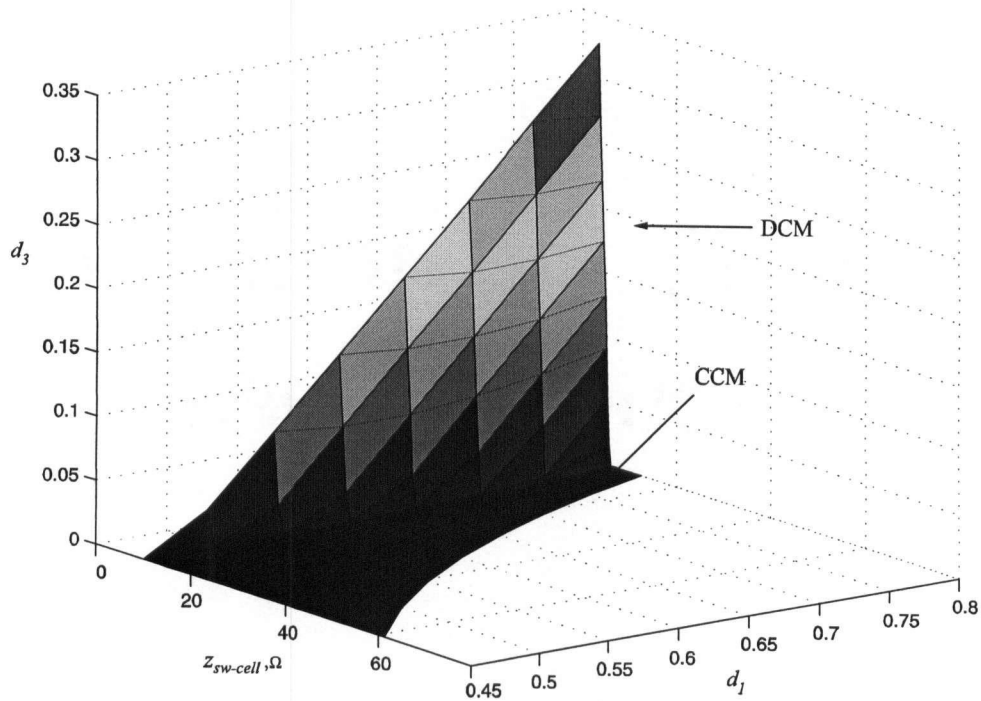
Fig. 4.21: Discontinuous subinterval d_3 in Cuk converter
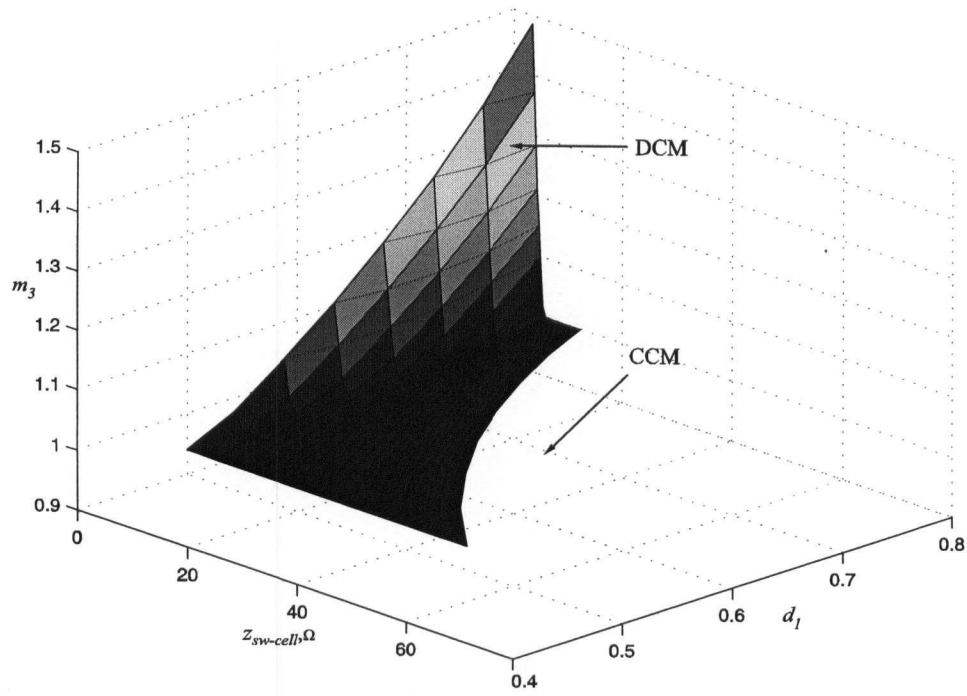
Fig. 4.22: Composite correction coefficient m_3 for the Cuk converter

4.4.2 Case study of cuk converter

The cuk converter in Fig . 33(a) with parameters summarized in Appendix B.6 is considered here. Also, the corresponding ASMG codes for the buck/boost converters are provided in Appendix C. 6. The cuk converter initially starts in CCM with a steady-state corresponding to the operating condition with $r_{Load} = 43\Omega$, $d_1 = 0.5$, and $v_g = 12V$. At $t = 0.001$ sec., another 8Ω resistor is connected in parallel to the load, changing the converter operational mode to discontinuous. Then, at $t = 0.003$ sec., the input voltage source is stepped up to 18V. The resulting overall time-domain transient is depicted in Fig. 4.23. As it can be seen in Fig. 4.23, the results produced by the developed average values model follow the transitions in operational modes and with excellent accuracy pass through the rippled waveforms produced by the detailed simulation.

The accuracy of proposed cuk converter model in frequency-domain has been verified by predicting the input-to-output small-signal transfer-function. The cuk converter is in DCVM , corresponding to the operating condition of $r_{Load} = 20\Omega$, $d_1 = 0.5$, and $v_g = 24V$. The transfer-function is evaluated up to 15 kHz. The resulting input-to-output transfer-function is

53

plotted in Fig. 4.24, where perfect match between the proposed and the detailed model is obtained.
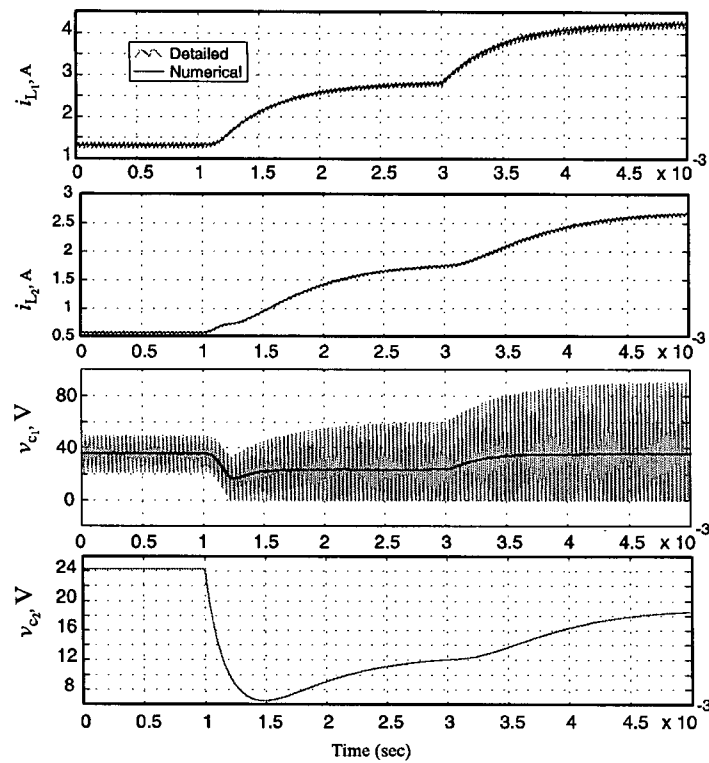
Fig. 4.23: Cuk converter inductor currents and capacitor voltages responses resulted from a step change in load followed by a step change in input voltage
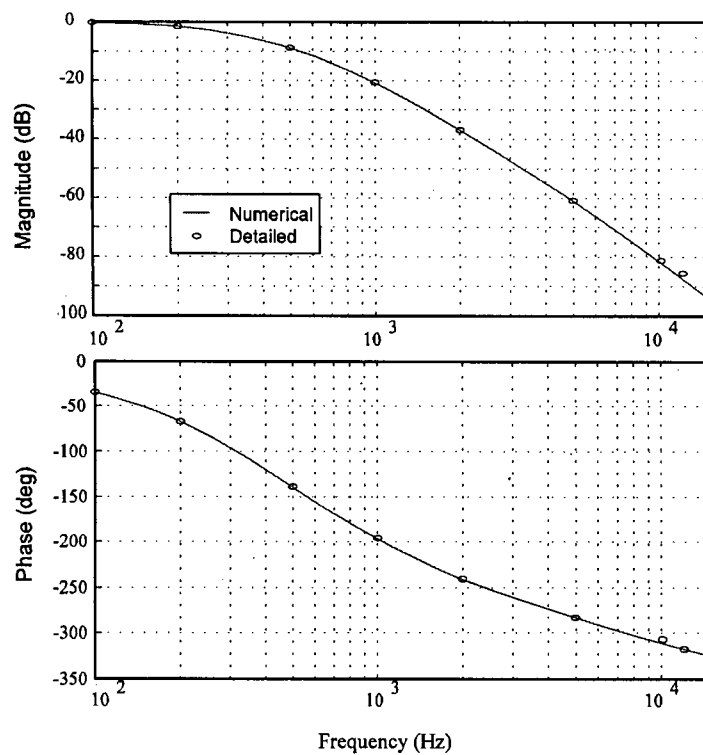
Fig. 4.24: Cuk converter input-to-output small-signal transfer-function

CHAPTER 5

Conclusion

5.1 Contribution

In this thesis, a new methodology for generating the average value models of PWM dc-dc converters is presented. The proposed methodology overcomes numerous challenges pertain to the previously developed techniques such as transition between modes, common averaging approximations, complexity of analytical derivations with the circuit parasitics, etc. It is shown that the key point of obtaining an accurate full-order averaged value model is to extract appropriate duty ratio constraint and correction term functions. The functions of the duty ratio constraint and correction terms are obtained numerically by running the detailed simulation in the range of interest. Even though establishing the proper averaged value model requires running the detailed simulation in a wide range of operating conditions, once established, the resulting model is continuous and valid for large-signal time-domain studies as well as for linearization and subsequent small-signal characterization of the overall system. Also, a fast algorithm to extract the small-signal characterization from a detail model is set forth. The proposed numerically averaged model is verified for basic PWM dc-dc converters in time- as well as frequency-domain against the hardware prototype, the detailed simulation and the analytical average value model.

5.2   Future work

The parametric average value modeling developed in this thesis provides a convenient framework to systematically average an arbitrary PWM dc-dc converter. This opens a new horizon for future research in the area of automated average value modeling of other power electronic converters. In particular, converter classes of interest include soft switching converters, resonant converters and current-mode converters, where the developed methodology can be extended with slight modifications. Furthermore, the obtained averaged models are suitable candidates for system-level studies concern with design, and stability investigation of complex power electronic systems. The application of this methodology to analysis of more complex converter systems will be addressed in future by the author.

Bibliography:

[1]   R. Tymerski, V. Vorperian, "Generation, classification and analysis of switched-mode DC-to-DC Converters by the use of switching cells," *in 1986 Proc. Int. Telecommunications Energy Conf.* (INTELEC'86), pp. 181-195, Oct. 1986

[2]   J. M. Burdio, A. Martinez, J. R. Garcia, "A synthesis method for generating switched electronic converters," *IEEE Trans. on Power Electronics*, vol. 13, No. 6, pp. 1056-1068, Nov. 1998

[3]   P. T. Krein, R. M. Bass, " Geometric Formulation, Classification and Methods for Power Electronics Systems," *PESC'90 records*, 21st annual IEEE meeting, pp. 499-505, June 11-14 1990

[4]   K. H. Liu, F. C. Lee, "Topological Constraints on basic PWM converters," *PESC'88 records*, 19th annual IEEE meeting, pp. 164-172, March 11th -14th , 1988

[5]   D. Maksimovic, S. Cuk, "General properties and synthesis of PWM DC-to-DC converters," *PESC '89 records*, 20th annual meeting, vol. 2, pp. 515-525, June 26th -29th , 1989

[6]   D. Maksimovic, "Synthesis of PWM and Quasi resonance dc-dc converters," Ph.D. thesis, California Institute of Technology, Jan. 1989

[7]   R. Venkataramanan, A. Sabanovic, S. Cuk, "Sliding mode control of dc-to-dc converters," *in IECON Conf. Proc.*, pp. 251-258, 1985

[8]   A. Kugi, K. Schacher, "Nonlinear H_∞ controller design for a dc-to-dc power converter," *IEEE Trans. on Control System Technology*, vol. 7, No. 2, March 1999

[9]   N. Femia, G. Spagnunolo, V. Tucci, "State-space Models and Order Reduction for DC-DC Switching Converters in Discontinuous Modes," *IEEE Trans. on Power Electronics*, vol. 10, No. 6, pp. 640-650 , Nov. 1995

[10]   T. Kato, G.C. Verghese, "Efficient Numerical Determination of Boundaries Between Operating Modes of Power Converter," *IEEE Workshop on Computer in Power Electronics*, pp. 205-216, 9-11 Aug. 1992

[11]   Y. Kuroe, T. Kato, N. Deguchi, "A Computer Aided Method for Determining Operating-Mode Boundaries in Power Electronic Circuits", *28th IEEE Power Electronics Specialists Conf. (PESC'97)*, vol. 2, pp. 1345–1351, 17-22 June 1997

[12] J. Jatskevich, O. Wasynczuk, E. A. Walters. C. E. Lucas, S. D. Pekarek, P. T. Lamm, "Automated Identification of the operational modes of switched electric circuits," *Power System Conf.*, San Diego, California, Oct. 31-Nov. 2, 2000

[13] D. Maksimovic, and S. Cuk, "A general approach to synthesis and analysis of quasi-resonance converters," *IEEE PESC '89 records,* pp. 713-727, 1989

[14] J. Chen, R. Erikson, D. Maksimovic, "Averaged switch modeling of boundary conduction mode dc-to-dc converters," in Proceedings *IECON'01*, 27th annual meeting of IEEE Industrial Electronic society, pp. 844-849, 2001

[15] Y. S. Lee, S. J. Wang, S. Y. R. Hui, "Modeling analysis and application of buck converters in discontinuous-input-voltage-mode," *IEEE Trans. on Power Electronics*, vol. 12, pp. 350-360, March 1997

[16] D. Sadarnac, W. Abida, C. Karimi, "The Double Discontinuous Conduction Mode Operation of a Converter: A method for Soft Switching," *IEEE Trans. on Power Electronics*, vol. 19, No. 2, March 2004

[17] K. Schenk, S. Cuk, "Small-signal analysis of converters with multiple discontinuous conduction modes," *29th IEEE Power Electronics Specialists Conf. (PESC'98)*, vol. 1, pp. 623–629, 17-22 May 1998

[18] D. Weng, S. Yuvarajan, "Constant-switching frequency ac-dc converter using second-harmonic-injection PWM ," *in Proc. APEC'95*, pp. 642-646, 1995

[19] J. sun, N. Freleke, H. Grotetollen, " Harmonic reduction techniques for single-switch three-phase boost rectifiers," *in Proc. IAS'96*, pp. 1225-1232, 1996

[20] M. J. Willers, M. G. Egan, J. M. D. Murphy, S. Daly, "A BIFRED converter with a wide load range," *in proc. IEEE IECON'94*, Bologna, Italy, pp. 226-231, 1994

[21] M. J. Willers, M. G. Egan, S. Daly, J. M. D. Murphy, "Analysis and design of a practical discontinuous-conduction-mode BIFRED converter," *IEEE Trans. on Industrial Electronics*, vol. 46, No. 4, Aug 1999

[22] G. Spiazzi, L. Rossetto, P. Mattavelli, S. Buso, "High-Quality Rectifier based on cuk converter in discontinuous capacitor voltage mode," Technical report, University of Padova, Italy

[23] B. T. Lin, Y. S. Lee, "Power-Factor correction using Cuk converters in Discontinuous-Capacitor-Voltage mode operation," *IEEE Trans. on Industrial Electronics,* vol. 44, No. 5, Oct. 1997

[24] D. S. L. Simonetti, J. Sebastian, J. Uceda, " The Discontinuous Conduction mode Sepic and Cuk Power Factor Preregulatrs: Analysis and Design," *IEEE Trans. on Industrial Electronics*, vol. 44, No. 5, Oct. 1997

[25] D. Weng, S. Yuvarjan, "Constant-switching frequency ac-dc converter using second-harmonic-injection PWM," *in Proc. of APEC'95*, pp. 642-646, 1995

[26] L. Jinjun, F. Xiaogang, F. C. Lee, D. Borojevich, "Stability margin monitoring for DC distributed power systems via perturbation approaches," *IEEE Trans. Power Electronics*, vol. 18, Iss. 6, pp. 1254-1261, Nov. 2003

[27] S. D. Sudhoff, S. Pekarek, B. Kuhn, S. Glover, J. Sauer, D. Delisle, "Naval combat survivability testbeds for investigation of issues in shipboard power electronics based power and propulsion systems," IEEE PES Summer Meeting, vol. 1, pp. 347-350, July 2002

[28] M. B. Harris, A. W. Kelley, J. P. Rhode, M. E. Baran, "Instrumentation for measurement of line impedance," *Conf. Proc. of Applied Power Electronics Conference* (APEC'94), vol.2, p. 887-893, 1994

[29] B. Palethorpe, M. Sumner, D. W. Thomas, "Power system impedance measurement using a power electronic converter," *Proc. 9th International Conference on Harmonics and Quality of Power*, vol. 1, p. 208-213, 2000

[30] *Advanced Continuous Simulation Language (ACSL)*, Reference Manual, Version 11, MGA Software, 1995

[31] *Simulink: Dynamic System Simulation for Matlab*, Using Simulink Version 5, The MathWorks Inc., 2003 (Simulink LTI Viewer)

[32] P. T. Krein, J. Bentsman, R. M. Bass, B. L. Lesieutre, "On the use of averaging for the analysis of power electronic systems," *IEEE Trans. Power Electronics*, vol. 5, Iss. 2, pp. 182-190, Apr. 1990

[33] S. Cuk, R. D. Middlebrook, "A general unified approach to modeling switching DC-to-DC converters in discontinuous conduction mode," *in Proc. IEEE PESC'77*, pp. 36–57, 1977

[34] D. Maksimovic, S. Cuk, *"A unified analysis of PWM converter in discontinuous mode," IEEE Trans. Power Electronics*, vol. 6, Iss. 3, pp. 476–490, July 1991

[35] R. W. Erikson, D. Maksimovic, *Fundamental of Power Electronics*, Kluwer academic publication, 2nd edition, 2001

[36] V. Vorperian, "Simplified analysis of PWM Converters using the model of PWM switches: Part I and II ," *IEEE Trans. Aerospace and Electronic Systems*, vol. AES-26, pp. 490-505, May 1990

[37] Jian Sun, D. M. Mitchell, M. F. Greuel, P. T. Krein, R. M. Bass, "Averaged modeling of PWM converters operating in discontinuous conduction mode," *IEEE Trans. Power Electronics*, vol. 16, Iss. 4, pp. 482–492, July 2001

[38] H. A. Owen, A. Capel, J. G. Ferrante. "Simulation and analysis methods for sampled power electronic systems," *in IEEE PESC '76*, pp. 44-55, 1976

[39] A. R. Brown, R. D. Middlebrook, "Sampled-data modeling of switching regulators," *in IEEE PESC'81*, pp. 349-369, 1981

[40] D. J. Shortt, F. C. Lee, "Extention of discrete-average models for converter power stages," *in IEEE PESC'83*, pp.23-37, 1983

[41] J. M. burdio, A. Matinez, "A unified discrete-time state-space model for switching converters," *IEEE Trans. on Power Electronics*, vol. 10, pp. 694-707, Nov. 1995

[42] P. Maranesi, "PWM converter characterization in the frequency-domain through fast time-domain computer simulation," in *Proc. 2nd Workshop Comput. Power Electron.*, 1990

[43] B. Y. Lau and R. D. Middlebrook, "Small-signal frequency response theory for piecewise - constant two-switched-network dc-to-dc converter systems," in *Proc. IEEE PESC 86*, pp. 186–200, 1986

[44] R. Tymerski, "On the efficacy of sampled data modeling of switched networks," *in Proc. 5th IEEE workshop Comput. Power Electron.* , pp.14-17, 1996

[45] G. W. Wester, R. D. Middlebrook, "Low-Frequency characterization of Switched DC-DC converters," *IEEE Trans. Aerospace and Electronic Systems*, vol. AES-9, pp. 376-385, May 1973

[46] J. M. Noworski, S. R. Sanders, "generalized in-place averaging," *in IEEE Applied Power Electronic Conf.*, pp. 445-451, 1991

[47] R. Tymerski, V. Vorperian, F. C. Lee, W. Baumann, "Nonlinear modeling of PWM switch," *IEEE PESC rec.*, 1988

[48] V. Vorperian. "Simplified analysis of PWM converters using model of PWM switch. II. Discontinuous conduction mode," *IEEE Trans. Aerospace and Electronic Systems*, vol. 26, Iss. 3, pp.497 – 505, May 1990

[49] R. Tymerski, V. Vorperian, "Generalization and classification of PWM DC-to-DC Converters," *IEEE Trans. Aerospace and Electronic Systems*, vol. 24, No. 6, pp. 743-750, Nov. 1988

[50] J. Sun, D. M. Mitchell, M. F. Greuel, P. T. Krein, R. M. Bass, "Modeling of PWM converters in discontinuous conduction mode; A reexamination," *29th IEEE Power Electronics Specialists Conf. (PESC'98)*, vol. 1, pp. 615–622, 17-22 May 1998

[51] D. Maksimovic, A. M. Stankovic, V. J. Thottuveil, G. C. verghese, "Modeling and simulation of Power Electronic Converters," *in Proc. of IEEE*, vol. 89, No. 6, June 2001

[52] Y. S. Lee, "A systematic and unified approach to modeling switches in switch-mode power supplies," *IEEE Trans on Industrial Electronics*, vol. IE-32, pp.445-448, Nov. 1985

[53] E. E. Landsman, "A unifying derivation of switching regulator topologies", *IEEE PESC'79*, pp. 239-243 , 1997

[54] S. R. Sanders, G. C. Verghese, "Synthesis of averaged circuit models for switched power converters," *IEEE Trans. Circuit and Systems*, vol. 38, pp. 905-915, Aug. 1991

[55] R. W. Brockett, J. R Wood, "Electrical networks containing controlled switches," *addendum to IEEE Symposium on Circuit Theory*, Apr. 1974

[56] S. R. Sanders, J. M. Noworolski, X. Z. Liu, G. C. Verghese, "Generalized averaging method for power conversion circuits," *IEEE Trans. Power Electronics*, vol. 6, Iss. 2, pp. 251–259, Apr. 1991

[57] S. R. Sandres, "On limit cycles and describing function method in periodically switched circuits," *IEEE Trans. Circuit Syst. 1*, vol. 40, pp. 564-572, Sept. 1993

[58] J. White, S. Leeb, "An envelope-following approach to switching power converter simulation," *IEEE Trans. Power Electron.*, vol. 6, pp.303-307, Apr. 1991

[59] V. A. Caliskan, G. C. Verghese, A. M. Stanlovic, " Multifrequency averaging of dc/dc converters," *IEEE Trans. Power Electron.*, vol .14, pp. 124-133, Jan 1999

[60] L. G. De Vicuna, F. Guinjoan, J. Majo, L. Martinez, "Discontinuous conduction mode in the SEPIC converter," *Electrotechnical Conf. Integrating Research, Industry and Education in Energy and communication Engineering*, pp. 38-42, 11-13 Apr. 1989

[61] A. Kislovski, R. Redl, N. Sokal, *Dynamic Analysis of Switching-Mode DC/DC Converters*, New York, Van Nostr and Reinhold, 1994

[62] J. G. Kassakian, M. F. Schecht, G. C. Verghese, *Principles of Power Electronics*, Addison-Wesley press, June 1992

[63] P. T. Krein, *Elements of Power Electronics*, New York, Oxford University Press, 1998

[64] A. Reatti, M. K. Kazimierczuk, "Small-signal model of PWM converters for discontinuous conduction mode and its application for boost converter," *IEEE Trans. Circuits and Systems I: Fundamental Theory and Applications*, vol. 50, Iss. 1, pp. 65–73, Jan. 2003

[65] R. Tymerski, "Application of time varying transfer-function for exact small-signal analysis, in *Proc. IEEE PESC'91*, pp. 80-87, 1991

[66] J. Groves, "Small-signal analysis using harmonic balance methods," in *Proc. IEEE PESC'91*, pp. 74-79, 1991

[67] J. Sun, H. Grotstollen, "Averaged modeling of switching power converters: Reformulation and theoretical basis," *IEEE Power Electronics Specialists Conf. (PESC'92)*, pp. 1165–1172, 1992

[68] Jian Sun, H. Grotstollen, "Symbolic analysis methods for averaged modeling of switching power converters," *IEEE Trans. Power Electronics*, vol. 12, Iss. 3, pp. 537-546 , May 1997

[69] S. B. Yaakov, D. adar, "Average models as tools for studying the dynamics of switch-mode dc-dc converters," *in Proc. IEEE PESC' 94*, pp. 1369-1376, 1994

[70] J. Sun, D. M. Mitchell, M. F. Greuel, P. T. Krein, R. M. Bass, " Averaged models for PWM converters in discontinuous conduction mode," *in Proc. HFPC'98*, 1998

[71] R. C. Wong, J. Groves, "An automated small-signal frequency-domain analyzer for general periodic-operating systems as obtained via time-domain simulation," *in Proc. IEEE PESC' 95*, pp. 801-808, 1995

[72] R. C. Wong, "Accelerated Convergence to the steady-state solution of Closed-loop regulated Switching-Mode Systems as obtained through simulation," *IEEE Power Electronic Specialists Conference Record, IEEE publication No. 87CH2459-6*, pp. 682-692, June 1987

[73] P. Huynh, B. H. Cho, "Empirical small-signal modeling of switching converters using PSpice," *in Proc. IEEE PESC' 95*, pp. 809-815, 1995

[74] D. Maksimovic, "Computer-aided small-signal analysis based on impulse response of dc/dc switching power converters," IEEE Trans. on Power Electronics, vol. 15, No. 6, Nov. 2000

[75] P. Pejovic, D. Maksimovic, "PETS- A simulation tool for power electronics", in Proc. 1996, *IEEE Workshop Comput. Power Electron.* pp. 1-8, 1996

[76] D. Maksimovic, "Automated steady-state analysis of switching power converters using a general-purpose simulation tool," *in Proc. IEEE PESC'97*, 1997

[77] P. Pejovic, D. Maksimovic, "Determination of network state in switching power converters," *26th IEEE Power Electronics Specialists Conf. (PESC '95)*, vol. 2, pp. 816–822, 18-22 June 1995

[78] L. O. Chua, P. M. Lin, *Computer-aided analysis of electronic circuit, Algorithms and computational technique*, Prentice-Hall, Englweed Cliffs, NJ, 1975

[79] J. Jatskevich, O. Wasynczuk, E. A. Walters, C. E. Lucas, "Continuous state-space modeling of switched electric networks," *Proc. of the 2000 IEEE Int. Conf. Control Applications*, pp. 902 – 907, 25-27 Sept. 2000

[80] J. Jatskevich, O. Wasynczuk, E. A. Walters, C. E. Lucas, "A globally continuous state-space representation of switched networks," *IEEE Canadian Conf. Electrical and Computer Engineering (CCECE2000)*, vol. 1, pp. 559–563, 7-10 March 2000

[81] T. F. Wu, Y. K. K. Chen, "Modeling PWM DC/C converters out of basic converter units," *IEEE Trans. on Power Electronics*, vol. 13, No. 5, Sep. 1998

[82] R. D. Middlebrook, S. Cuk, "A general unified approach to modeling switching converter power stages," *8th IEEE Power Electronics Specialists Conf. (PESC'76)*, pp. 18-35, 8-10 June 1976

[83] E. A. Walters, "Automated averaging techniques for power-electronic-based systems," Ph.D. thesis, Purdue university, Oct. 1999

[84] S. B. Yakoov, D. Wulich, and W. M. Policka, "Resolution of an averaging paradox in the analysis of switched-mode dc-dc converters," *IEEE Trans. Aerosp. Electron. Syst.*, vol. 30, pp. 626-632, Apr. 1994

[85] G. C. Verghese, M. I. Spong, J. H. Lang, "Modeling and control challenges in power electronics,", *in Proceedings of 25th conference on decision and control*, pp.39-45, Dec. 1986

[86] W. M. Polivka, P. R. K. Chetty, R. D. Middlebrook, "State-space average modeling of converters with parasitics and storage-time modulation," *11th IEEE Power Electronics Specialists Conf. (PESC'80)*, pp. 119-145, 18-20 June 1980

[87] G. Nirguade, R. Tirumala, N. Mohan, "A new, large-signal average model for single-switch dc-dc converters operating in both CCM and DCM, " *32nd IEEE Power Electronics Specialist Conf. (PESC'01)*, vol. 3, pp. 1736-1741, 17-21 June 2001

[88] Chen Jingquan, D. Maksimovic, R. Erickson, "Buck-boost PWM converters having two independently controlled switches," *32nd IEEE Power Electronics Specialists Conf. (PESC'01)*, vol. 2, pp. 736-741, 17-21 June 2001

[89] N. Femia, G. Spagnuolo, M. Vitelli, "Steady-state analysis of soft-switching converters," *IEEE Trans. Circuits and Systems I: Fundamental Theory and Applications*, vol. 49, Iss. 7, pp. 939–954, July 2002

[90] *Automated State Model Generator(ASMG)*, Reference Manual, Version 2, PC Krause and Associates Inc., March 2002

[91] W. M. Polivka, P. R. K. Chetty, R. D. Middlebrook, "State-space average modeling of converters with parasitics and storage-time modulation," *11th IEEE Power Electronics Specialists Conf. (PESC'80)*, pp. 119-145, 18-20 June 1980

[92] A. Reatti, "Steady-state analysis including parasitic components and switching losses of buck and boost dc–dc converters under any operating condition," *Int. J. Electron.*, vol. 77, No. 5, pp. 679–702, 1994

[93] C. T. Rim, G. B. Joung, G. H. Cho, "Practical switch based state-space modeling of DC-DC converters with all parasitics," *IEEE Trans. Power Electronics*, vol. 6, Iss. 4, pp. 611-617, Oct. 1991

[94] J. M. Zhang, X. G. Xie, D. Z. Jiao, Zhaming Qian, "Stability problems and input impedance improvement for cascaded power electronic systesms," *APEC' 04*, 19th Annual IEEE, vol. 2, pp. 1018 - 1024, 2004

[95] S. D. Sudhoff, S. F. Glover, P. T. Lamm, D. H. Schmucker, D. E. Delisle, S. P. Karatsinides, "Admittance space stability analysis of power electronic systems," *IEEE Trans. on Aerospace and Electronic Systems*, vol. 36 , Iss. 3 , July 2000

[96] A. Emadi, "Modeling, Analysis and stability assessment of multi-converter power electronic systems," Ph.D. thesis, Texas A&M university, Dec. 2000

[97] B. G. Dobbs, P. L. Chapman, "A Multiple-Input DC-DC Converter Topology," *IEEE Power Electronics Letters*, vol. 1, No. 1, pp. 6-9, March 2003

Appendix

Appendix A : The fundamental approximation in the state-space averaging approach

Let the two linear systems be described by

$$\begin{cases} 0 \leq t < d_1 T_S & \dot{\mathbf{x}} = \mathbf{A}_1 \mathbf{x} \\ d_1 T \leq t < T_S & \dot{\mathbf{x}} = \mathbf{A}_2 \mathbf{x} \end{cases}$$

The exact solutions of these state-space equations are

$$\begin{cases} 0 \leq t < d_1 T_S & \mathbf{x}(t) = e^{\mathbf{A}_1 t} \mathbf{x}(0) \\ d_1 T \leq t < T_S & \mathbf{x}(t) = e^{\mathbf{A}_2 (t - d_1 T_s)} \mathbf{x}(d_1 T_s) \end{cases}$$

The state variable is continuous across the switching instance $d_1 T_s$:

$$\begin{cases} \mathbf{x}(T_s) = e^{\mathbf{A}_2 (T_s - d_1 T_s)} \mathbf{x}(d_1 T_s) = e^{\mathbf{A}_2 d_2 T_s} e^{\mathbf{A}_1 d_1 T_s} \mathbf{x}(0) \\ d_2 = 1 - d_1 \end{cases}$$

If the two matrixes $\mathbf{A}_1$ and $\mathbf{A}_2$ are commutative ($\mathbf{A}_1 \mathbf{A}_2 = \mathbf{A}_2 \mathbf{A}_1$) then using the first approximation of Baker-Campbell-Hausdorff results:

$$\begin{cases} e^{\mathbf{A}_1 d_1 T_s} \approx \mathbf{I} + d_1 \mathbf{A}_1 T_s \\ e^{\mathbf{A}_2 d_2 T_s} \approx \mathbf{I} + d_2 \mathbf{A}_2 T_s \end{cases} \Rightarrow e^{\mathbf{A}_2 d_2 T_s} e^{\mathbf{A}_1 d_1 T_s} \approx \mathbf{I} + (d_1 \mathbf{A}_1 + d_2 \mathbf{A}_2) T_s \approx e^{(d_1 \mathbf{A}_1 + d_2 \mathbf{A}_2) T_s}$$

Therefore, the final equation for the state variable is

$$\mathbf{x}(t) = e^{(d_1 \mathbf{A}_1 + d_2 \mathbf{A}_2) T_s} \mathbf{x}(0)$$

Which is the same as the solution of linear system:

$$\dot{\mathbf{x}} = (d_1 \mathbf{A}_1 + d_2 \mathbf{A}_2) \mathbf{x}$$

This continuous equation is the average model obtained from two switched equations.

Appendix B: The converters circuit parameters

B.1: Boost converter parameters

$v_g = 4V$, $r_{source} = 0.1\Omega$, $L = 6.2\mu H$, $r_L = 0.076\Omega$, $r_{sw} = 0.2\Omega$ (series resistance of MOSFET, IRFZ20), $f_s = 50kHz$, $v_d(on) = 0.4V$ (diode 12TQ035 forward voltage drop), $C = 14.2\mu F$, $r_c = 13.8k\Omega$

B.2: Buck converter parameters

$v_g = 12V$, $L = 40\mu H$, $r_L = 0.3\Omega$, $r_{sw} = 0.2\Omega$ (series resistance of MOSFET, IRFZ20), $f_s = 50kHz$, $C = 20\mu F$, $r_c = 15k\Omega$

B.3: Buck/boost converter parameters

$r_{source} = 0.1\Omega$, $L = 8\mu H$, $r_L = 0.076\Omega$, $r_{sw} = 0.17\Omega$ (series resistance of MOSFET, IRFZ20), $f_s = 100kHz$, $v_d(on) = 0.4V$ (diode 12TQ035 forward voltage drop), $C = 4.7\mu F$, $r_c = 15k\Omega$

B.4: System parameters of boost converter fed by buck converter

$v_{in} = 10V$, $r_{source} = 0.1\Omega$, $L_1 = 470\mu H$, $r_{L_1} = 0.5\Omega$, $r_{sw} = 0.2\Omega$ (series resistance of MOSFET, IRFZ20), $f_{s_1} = 5kHz$, $v_d(on) = 0.4V$ (diode 12TQ035 forward voltage drop), $C_1 = 47\mu F$, $r_{c_1} = 15k\Omega$, $L_2 = 6.2\mu H$, $r_{L_2} = 0.076\Omega$, $f_{s_2} = 50kHz$, $C_2 = 14.2\mu F$, $r_{c_2} = 13.8k\Omega$

B.5: Rectifier fed buck converter parameters

$v_{in} = 12V$, $\omega_s = 10000\pi$, $r_s = 0.1\Omega$, $L_s = 10\mu H$, $r_{L_f} = 0.2\Omega$, $C_f = 20\mu F$, $L_f = 47\mu H$, $r_{sw} = 0.2\Omega$, (series resistance of MOSFET, IRFZ20), $f_s = 50kHz$, $v_d(on) = 0.4V$ (diode 12TQ035 forward voltage drop), $C = 20\mu F$, $L = 40\mu H$, $r_c = 15k\Omega$

B.6: Cuk converter parameters

$v_g = 12V$, $r_s = 0.1\Omega$, $r_{L_1} = 1\Omega$, $L_1 = 2mH$, $C_1 = 470nF$, $r_{c_1} = 15k\Omega$, $r_{sw} = 0.2\Omega$ (series resistance of MOSFET, IRFZ20), $f_s = 30kHz$, $v_d(on) = 0.4V$ (diode 12TQ035 forward voltage drop), $C_2 = 22\mu F$, $r_{L_2} = 1\Omega$, $L_2 = 6.3mH$, $r_{c_2} = 30k\Omega$

Appendix C: The circuits ASMG codes

C.1: Boost converter ASMG code

```
function h = boost
% Define a model handle
h = 1;
start_br_list(h);
% System parameters are
L=6.2*1e-6;
rL1=0.176;%Inductor +source
rsw=0.17;
% Syntax of use the BRANCH function.
% # hdl br p n r L/C E/J
% # 1 2 3 4 5 6 7
L_branch(h, 1, 2, 1, 0, 0, 1);
L_branch(h, 2, 2, 3, rL1, L, 0);
L_branch(h, 3, 3, 4, rsw, 0, 0);
S_branch(h, 4, 4, 1, 2, 1);
S_branch(h, 5, 3, 5, 2, 0);
L_branch(h, 6, 5, 1, 0, 0, 1);
```

C.2: Buck converter ASMG code

```
function h = buck
% Define a model handle
h = 1;
start_br_list(h);
% System parameters are
L=470*1e-6;
```

```
% Syntax of use the BRANCH function.
% # hdl br p n r L/C E/J
% # 1 2 3 4 5 6 7
L_branch(h, 1, 2, 1, 0, 0, 1);
L_branch(h, 2, 2, 3, 0.2, 0, 0);
S_branch(h, 3, 3, 4, 2, 1);
S_branch(h, 4, 1, 4, 2, 0);
L_branch(h, 5, 4, 5, 0.5, L, 0);
L_branch(h, 6, 5, 1, 0, 0, 1);
```

C.3: Single phase rectifier ASMG code

```
function h = spdhbr
% Define a model handle
h = 2;
start_br_list(h);
% System parameters are
wb=377.0;
Ls1 = 1e-5;
rs1 = 0.1;
Lf2 = 47e-6;
rs2 = 0.1;
% Syntax of use the BRANCH function
% # hdl br p n r L/C E/J
% # 1 2 3 4 5 6 7
L_branch(h, 1, 2, 1, rs1, Ls1, 1);
S_branch(h, 2, 2, 3, 2, 0); % diode 1
S_branch(h, 3, 1, 3, 2, 0); % diode 2
S_branch(h, 4, 4, 2, 2, 0); % diode 3
S_branch(h, 5, 4, 1, 2, 0); % diode 4
L_branch(h, 6, 3, 5, rs2, Lf2, 0);
L_branch(h, 7, 5, 4, 0, 0, 1); % cap
```

C.4: Buck converter ASMG code

```
function h = buck
% Define a model handle
h = 1;
start_br_list(h);
% System parameters are
L=40*1e-6;
% Syntax of use the BRANCH function.
% # hdl br p n r L/C E/J
% # 1 2 3 4 5 6 7
L_branch(h, 1, 2, 1, 0, 0, 1);
L_branch(h, 2, 2, 3, 0.2, 0, 0);
S_branch(h, 3, 3, 4, 2, 1);
S_branch(h, 4, 1, 4, 2, 0);
L_branch(h, 5, 4, 5, 0.3, L, 0);
L_branch(h, 6, 5, 1, 0, 0, 1);
```

C.5: Buck/boost converter ASMG code

```
function h = buck_boost
% Define a model handle
h = 1;
start_br_list(h);
% System parameters are
L=8*1e-6;
% Syntax of use the BRANCH function.
% # hdl br p n r L/C E/J
% # 1 2 3 4 5 6 7
L_branch(h, 1, 2, 1, 0, 0, 1); % source branch
S_branch(h, 2, 2, 3, 2, 1);; % stator branch
L_branch(h, 3, 3, 4, 0.17, 0, 0); % stator branch
```

```matlab
L_branch(h, 4, 4, 1, 0.176, L, 0); % controllable switch
S_branch(h, 5, 5, 4, 2, 0); % diode
L_branch(h, 6, 5, 1, 0, 0, 1); % source branch
```

C.6: Cuk converter ASMG code

```matlab
function h = cuk
% Define a model handle
h = 1;
start_br_list(h);
% System parameters are
L1 = 2000e-6;
L2 = 6800e-6;
C1 = 470*1e-9;
% Syntax of use the BRANCH function.
% # hdl br p n r L/C E/J
% # 1 2 3 4 5 6 7
L_branch(h, 1, 2, 1, 0, 0, 1);
L_branch(h, 2, 2, 3, 1, L1, 0);
S_branch(h, 3, 3, 1, 2, 1);
C_branch(h, 4, 3, 4, 15000, C1, 0);
S_branch(h, 5, 4, 1, 2, 0);
L_branch(h, 6, 5, 4, 1, L2, 0);
L_branch(h, 7, 5, 1, 0, 0, 1);
```

Vita

Ali Davoudi (IEEE St.M'04) received the B.S.E.E from Sharif University of Technology, Tehran, Iran, in 2003. He is presently a graduate student in the department of Electrical and Computer Engineering at the University of British Columbia, Vancouver, Canada. His research interests include power electronics, power electronic-based systems, energy conversion systems and power quality.